Investigation of the Relation between the Spectral Energy Distributions and the Emission Lines in Low#Redshift Quasars

THE ASTROPHYSICAL JOURNAL, 513:76–107, 1999 March 1

INVESTIGATION OF THE RELATION BETWEEN THE SPECTRAL ENERGY DISTRIBUTIONS AND EMISSION LINES IN LOW-REDSHIFT QUASARS[1]

BELINDA J. WILKES, JOANNA KURASZKIEWICZ,[2] PAUL J. GREEN, SMITA MATHUR, AND JONATHAN C. MCDOWELL
Harvard-Smithsonian Center for Astrophysics, Cambridge, MA 02138
Received 1997 December 23; accepted 1998 October 6

ABSTRACT

We investigate the relations between the observed emission-line strengths, widths, and continuum properties of a sample of 41 low-redshift ($z < 1$) quasars for which contemporaneous IR/soft X-ray spectral energy distributions are available. This includes investigating correlations between optical and UV lines with both the luminosity and the shape of the quasars' continuum, as well as correlations between the various lines. The sample is heterogeneous, primarily selected on the existence of good-quality *Einstein* X-ray data, and includes 18 radio-loud and 23 radio-quiet quasars. We find anticorrelations between the equivalent width and various UV luminosities (the Baldwin effect) for the Lyα and Hβ lines and a marginal anticorrelation for C III]. Exclusion of narrow-line, low-luminosity active galactic nuclei reveals a significant Baldwin effect for the C IV and C III] lines. A significant anticorrelation of EW(C IV) with α_{ox} is also present. We find no correlations between any lines and the X-ray luminosity or X-ray slope. The Fe II optical multiplet shows no simple relationship with luminosity or continuum slope; however, there is a tendency for objects with flat X-ray spectra and/or strong X-ray luminosities to have weak Fe II.

Our data do not favor a model in which changes in continuum shape (due to, e.g., a decreasing ionization parameter) cause the Baldwin effect. The data can instead be explained by an accretion disk (AD) model in which limb darkening and the projected surface area of an optically thick, geometrically thin disk combine to cause a viewing-angle–dependent UV luminosity and a more isotropic X-ray luminosity. The scatter in our correlations is larger than that expected from this AD model, suggesting the presence of dust, which reddens both the continuum and the broad emission lines. The C IV and C III] lines show flatter slopes and larger scatter in the line-continuum relations than predicted by the AD + dusty torus model. This may be due to a significant contribution from collisional excitation that is not directly related to the ionizing continuum.

Subject headings: galaxies: active — quasars: emission lines — quasars: general

1. INTRODUCTION

The strong, broad emission lines that characterize quasar spectra are generally believed to be generated in a large number of small gas clouds photoionized by the central continuum source of a quasar. This region is known as the broad emission line region (BELR). To date, photoionization models have been reasonably successful in predicting the average emission-line properties of a quasar using an average continuum shape. However, it has become clear that, while the emission-line properties are largely similar from quasar to quasar, the observed spectral energy distributions (SEDs) are not (Elvis et al. 1994, hereafter E94). If photoionization models are generally applicable, we would expect systematic relations between the observed lines and continuum in different objects (Krolik & Kallman 1988) and, at first glance at least, the dichotomy between continuum and the line behavior looks surprising.

The most enduring relation between the lines and continua in quasars is the inverse correlation between line equivalent width (EW) and continuum luminosity, known as the Baldwin effect (Baldwin 1977). This relation is not predicted in a simple photoionization scenario, and explanations range from luminosity-dependent continuum shape, which affects the BELR ionization, to geometric effects. Another intriguing set of correlations, which have caused a flurry of activity in recent years, centers around an inverse relation between the strengths of the broad Fe II λ4570 and narrow [O III] λ5007 lines and includes soft X-ray slope and luminosity and broad line width (Boroson & Green 1992; Boller, Brandt, & Fink 1996; Lawrence et al. 1997). Again, a simple photoionization scenario fails. The current popular explanation involves the mass flow into the central black hole; this is attractive, as it would imply an observational link into the central power house (Pounds, Done, & Osbourne 1996). Despite the general success of photoionization models, these results suggest that other factors also play a role in determining the emission-line properties of quasars.

Most studies of line and continuum properties of quasars to date have centered around large samples, often including nonuniform data sets from a variety of sources and generally utilizing global continuum parameters such as L_{opt}, L_x and α_{ox}. Since the photoionization of any individual ion and its resulting relation with the ionizing continuum is unique to that ion, the use of global parameters has obvious limitations for investigating photoionization models. The current study takes a different, complementary approach in concentrating on uniform, high-quality continuum and emission-line data for a small sample of quasars. This data set facilitates a study of the relation of each emission line to various parts of the continuum and, potentially, allows differentiation between ionization and other effects.

[1] Observations reported here were obtained at the Multiple Mirror Telescope Observatory, a facility operated jointly by the University of Arizona and the Smithsonian Institution.

[2] Also N. Copernicus Astronomical Center, ul. Bartycka 18, 00-716 Warsaw, Poland.

We have obtained far-IR through soft X-ray (100 μm–3.5 keV) continuum data for a sample of 41 quasars. SEDs for 30 of these objects were presented in E94; the remaining 11 are compiled here from a combination of our own and published data. We also present low-resolution (5–20 Å) optical spectrophotometry that was obtained within a few months of the optical/IR continuum measurements. UV spectra from *IUE* and/or the *Hubble Space Telescope* (*HST*) have been obtained either by ourselves or from their respective archives. The range in shapes of the IR–UV continuum is large even in this small, low-redshift sample (E94), allowing investigation of whether the range in continuum shapes produces any corresponding range in the emission-line properties.

2. OBSERVATIONS AND DATA REDUCTION

2.1. *The Sample*

Our sample is a heterogeneous sample of 41 low-redshift quasars ($z < 1$), where 23 are radio quiet (RQQ) and 18 are radio loud (RLQ). The radio-quiet objects dominate at lower redshifts, while the radio-loud dominate at higher redshifts (see Fig. 1). All but three quasars (PG 1012+008, PG 1121+422, and PG 2304+042) have *Einstein* X-ray observations with sufficient counts to define the X-ray spectral index. This selection introduces a bias toward objects with strong X-ray emission relative to the optical (small α_{ox}). The SEDs for 30 objects were presented in E94. For the remaining 11 objects the SEDs were assembled from existing data as described below. The list of all quasars with their redshifts is given in Table 1.

2.2. *Optical Spectroscopy*

The quasars were observed during the period 1985–1991 mostly with the Multiple Mirror Telescope (MMT) on Mount Hopkins in Arizona. Both blue and red spectrographs were used as far as possible to provide full coverage (3200–8400 Å) of the optical continuum. Southern objects were observed with the Cerro Tololo Inter-American Observatory (CTIO) 1.5 m telescope and CCD spectrograph. The observational details are given in Table 1, including the instrument and wavelength range covered in each case.

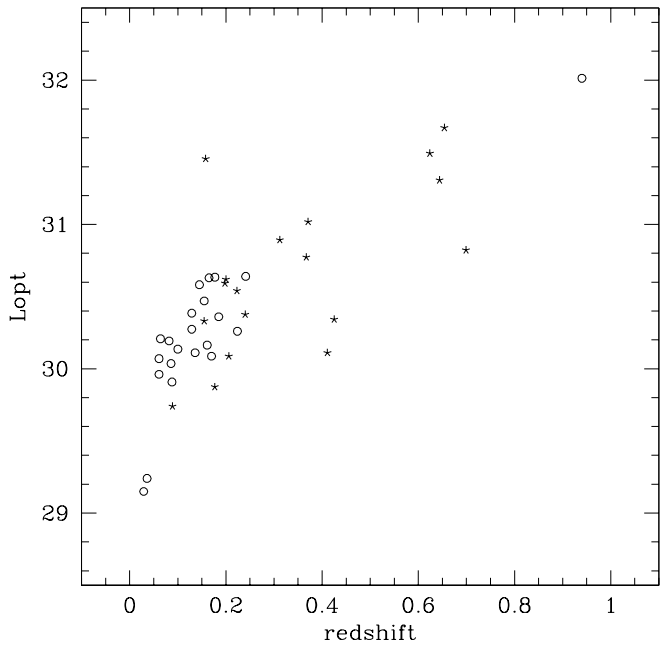

FIG. 1.—L_{opt} (2500 Å luminosity) vs. redshift for our sample. In this and all subsequent figures, stars indicate RLQs and circles RQQs.

In photometric conditions, spectrophotometry was carried out by observing each quasar twice, first through a large aperture, $\gtrsim 5''$, and second through a small aperture, $\sim 1''.5$, for a longer time in order to obtain high spectral resolution and signal-to-noise ratio (S/N). A standard star was observed through the wide aperture, at similar air mass, immediately before or after the quasar observation to provide flux calibration. The data were reduced in the standard manner using IRAF. The continuum of the small aperture data was then normalized to match the shape and absolute flux level of the large aperture observation, yielding a final spectrum with resolution $\sim$5–20 Å (depending on the instrument) and a photometric accuracy of $\sim$5%. Except where noted in Table 1, all spectra have been flux calibrated using a large-aperture spectrum and observed in photometric conditions as described above. The date of the spectrophotometry, sometimes different from that of the higher S/N, small-aperture spectrum, is also noted in Table 1.

In some cases several spectra covering largely overlapping wavelength ranges were obtained. If no significant change in continuum shape was apparent, these spectra were combined to improve the final S/N. Spectra with continuum shapes that did not agree within the errors were not combined, instead the discrepant or lower quality spectrum was discarded. Blue and red spectra of the same object were not combined since this adds uncertainty in the small overlap region of the spectra and is not required for our analysis. Table 1 lists observational details for all the individual spectra (i.e., before being combined). The final, combined spectra are presented in Figure 2 in order of increasing right ascension with blue and red spectra displayed separately.

The fluxes, EW, and FWHM were measured for all the prominent optical and UV emission lines: O VI λ1034 + Lyβ λ1025, Lyα λ1216 + N V λ1240, Si IV λ1397 + O IV] λ1402, C IV λ1549, C III] λ1909 + Si III] λ1892 + Al III λ1857, Mg II λ2798, [Ne V] λ3426, [O II] λ3727, [Ne III] λ3869 + He I λ3889, [Ne III] λ3967, Hδ λ4102, Hγ λ4340, Fe II λ4570, Hβ λ4861, and [O III] λ5007. The EW and fluxes were measured by the summation procedure detailed in Robertson (1986), which provides a better estimate of the line wings than Gaussian fitting. All fluxes and EW were remeasured using the SPLOT task in IRAF. Rather than fitting a Gaussian function to these lines, which frequently does not work well, we measured the actual data by fitting a linear continuum and integrating across the observed emission line. If the EW and fluxes derived by both methods agreed within 10%, the values obtained by the summation procedure were used for the subsequent analysis. If they disagreed, the values from the SPLOT task were used. For the Fe II optical multiplet, which is especially difficult to measure if the line is weak, the summation procedure was used to determine the EW. The FWHMs were measured using only the IRAF SPLOT task by fitting a linear continuum, measuring the line peak flux above the continuum, determining the half-maximum intensity, and measuring the width at that level. By measuring all the data ourselves, we minimize the scatter generally introduced by

TABLE 1

OBSERVATIONAL DETAILS

Name	α(J2000)	δ(J2000)	z	UT Date	Telescope Instrument[a]	λ Range (Å)	Δλ (Å)	Time (s)	Flux Date[b]
III Zw 2[e]	00 10 30.98	+10 58 29.4	0.089	1987 Dec 15	MMT/BB	3200–6400	6	2400	1989 Jan
PG 0026+129[e]	00 29 13.8	+13 16 04.0	0.145[d]	1987 Oct 27	MMT/BB	3200–6400	6	2400	1989 Jan
0044+030	00 47 05.7	+03 19 57.1	0.624	1987 Dec 16	MMT/BB	3200–6400	6	1200	...
I Zw 1[e]	00 53 34.9	+12 41 36.3	0.061	1991 Sep 16	MMT/RC	3680–8780	20	240	1991 Sep
PHL 909[e]	00 57 09.91	+14 46 11.2	0.17	1987 Oct 27	MMT/BB	3200–6400	6	1800	1988 Jan
3C 47	01 36 24.4	+20 57 27.7	0.425	1989 Jan 10	MMT/BB	3500–6400	6	2400	1989 Jan
3C 48[e]	01 37 49.8	+32 54 20.4	0.367	1987 Oct 27	MMT/BB	3200–6400	6	3000	1988 Jan
				1987 Dec 16	MMT/BB	3200–6400	6	1800	1988 Jan
NAB 0205+024[e]	02 07 49.9	+02 42 55.9	0.155	1987 Oct 27	MMT/BB	3200–6400	6	2400	1988 Jan
				1985 Oct 14	MMT/FGS	4200–7400	10	1000	...
				1991 Sep 16	MMT/RC	3680–8780	20	600	1991 Sep
PKS 0312−770[e]	03 11 54.7	−76 51 51.4	0.223	1989 Feb 27	CTIO	5000–9500	20	2700	1989 Feb
PKS 0637−752[e]	06 35 46.5	−75 16 17.1	0.651	1989 Feb 27	CTIO	5000–9500	20	3150	1989 Feb
PG 0804+761[e]	08 47 42.46	+34 45 04.6	0.100	1989 Jan 10	MMT/BB	3500–6400	6	1800	1988 Jan
3C 206[e]	08 39 50.6	−12 14 33.8	0.198	1988 Apr 09	MMT/FGS	4500–8400	10	900	1988 Apr
PG 0844+349[e]	08 47 42.46	+34 45 04.6	0.064	1987 Dec 16	MMT/BB	3200–6400	6	1200	1987 Dec
				1987 Mar 01	MMT/BB	3150–6300	6	1200	1987 Mar
3C 215	09 06 32.00	+16 46 12.0	0.411	1988 Jan 11, 12	MMT/BB	3200–6400	6	4800	1987 Dec
Mrk 704[e]	09 18 26.0	+16 18 19.7	0.029	1989 Feb 28	CTIO	5000–9500	20	900	1989 Feb
0923+392	09 23 55.3	+39 15 24	0.699	1987 Dec 16	MMT/BB	3200–6400	6	3600	1987 Dec
PG 1001+054	10 04 20.09	+05 13 00.5	0.161	1989 Jan 10	MMT/BB	3200–6400	6	2400	1989 Jan
				1989 Feb 28	CTIO	5000–9500	20	2400	1989 Feb
PG 1004+130	10 07 26.1	+12 48 56.4	0.241	1989 Feb 27	CTIO	5000–9500	20	1350	1989 Feb
PG 1012+008	10 14 54.90	+00 33 37	0.185	1987 Dec 15	MMT/BB	3200–6400	6	1200	1987 Dec
				1988 Apr 08	MMT/FGS	4500–8400	10	900	1988 Apr
B2 1028+313[e]	10 30 59.10	+31 02 55.5	0.177	1988 Jan 11, 12	MMT/BB	3200–6400	6	3000	1987 Dec
				1988 Apr 09	MMT/FGS	4500–8400	10	900	1988 Apr
3C 249.1[e]	11 04 13.84	+76 58 57.6	0.313	1988 Jan 13	MMT/BB	3200–6400	6	1800	1988 Jan
				1987 Mar 03	MMT/BB	3200–6400	6	1200	1988 Jan
				1988 Jun 12	MMT/BB	3200–6400	6	1800	1988 Jan
PG 1116+215[e]	11 19 08.66	+21 19 17.8	0.177	1988 Jan 12	MMT/BB	3200–6400	6	1200	1988 Jan
				1987 Mar 03	MMT/BB	3150–6300	6	720	1987 Mar
				1988 Apr 09	MMT/FGS	4500–8400	10	600	1988 Apr
PG 1121+422	11 24 35.5	+42 00 24.9	0.224	1988 Jan 13	MMT/BB	3200–6400	6	2400	1988 Jan
				1987 Mar 03	MMT/BB	3150–6300	6	1800	1987 Mar
3C 263[e]	11 39 57.07	+65 47 49.6	0.652	1988 Jan 13	MMT/BB	3200–6400	6	1200	1988 Jan
GQ Comae[e]	12 04 42.17	+27 54 11.7	0.165	1989 Jan 31	MMT/BB	3200–6400	6	1200	...
PG 1211+143[e]	12 14 17.60	+14 03 12.5	0.080[d]	1988 Jan 13	MMT/BB	3200–6400	6	480	1988 Jan
				1988 Jun 07	MMT/BB	3200–6400	6	1200	1988 Jun
				1987 Mar 03	MMT/BB	3150–6300	6	960	1987 Mar
				1988 Apr 09	MMT/FGS	4500–8400	10	300	1988 Apr
PKS 1217+023	12 20 11.9	+02 03 42.3	0.240	1988 Jun 11	MMT/BB	3200–6400	6	1800	1988 Jun
3C 273[e]	12 29 06.7	+02 03 08.6	0.158	1988 Apr 09	MMT/FGS	4500–8400	10	300	1988 Apr
				1988 Jun 12	MMT/BB	3200–6400	6	1800	1988 Jun
PG 1307+085[e]	13 09 47.04	+08 19 49.5	0.155	1988 Jun 07	MMT/BB	3200–6400	6	1800	1988 Jun
				1987 Mar 03	MMT/BB	3150–6300	6	1200	1987 Mar
				1988 Apr 09	MMT/FGS	4500–8400	10	600	1988 Apr
PG 1351+640	13 53 15.82	+63 45 44.4	0.087	1989 Jan 10	MMT/BB	3200–6400	6	2000	1989 Jan
PG 1407+265[c,e]	14 09 23.00	+06 18 20.65	0.944	...	...	...	...	...	...
PG 1416−129[e]	14 19 03.83	−13 10 44.8	0.129	1988 Jun 11	MMT/BB	3200–6400	6	2200	1988 Jun
				1988 Apr 09	MMT/FGS	4500–8400	10	900	1988 Apr
PG 1426+015[e]	14 29 06.59	+01 17 06.2	0.086	1988 Jun 7, 11	MMT/BB	3200–6400	6	2400	1988 Jun
				1988 Apr 09	MMT/FGS	4500–8400	10	900	1988 Apr
Mrk 841[e]	15 04 01.18	+10 26 16.13	0.036	1988 Jun 11	MMT/BB	3200–6400	6	2200	1988 Jun
PG 1613+658[e]	16 13 57.26	+65 43 10.2	0.129	1990 Oct 16	MMT/BB	3200–6400	6	1440	...
				1988 Jun 12	MMT/BB	3200–6400	6	1420	1988 Jun
				1988 Apr 09	MMT/FGS	4500–8400	10	720	1988 Apr
3C 351[e]	17 04 41.37	+60 44 30.26	0.371	1988 Jun 12	MMT/BB	3200–6400	6	1440	1988 Jun
				1988 Apr 09	MMT/FGS	4500–8400	10	720	1988 Apr
1721+343[e]	17 23 20.8	+34 17 58.4	0.206	1987 Oct 27	MMT/BB	3200–6400	6	1200	...
KAZ 102[e]	18 03 28.85	+67 38 09.6	0.136	1990 Oct 13, 16	MMT/BB	3200–6400	6	1200	1990 Oct
				1988 Jun 11	MMT/BB	3200–6400	6	1140	1988 Jun
				1988 Apr 09	MMT/FGS	4500–8400	10	720	1988 Apr
II Zw 136[e]	21 32 27.94	+10 08 17.4	0.061	1987 Oct 26	MMT/BB	3200–6400	6	1800	1987 Oct
PHL 1657[e]	21 37 45.2	−14 32 55.4	0.200	1985 Oct 14	MMT/FGS	4200–7400	10	1200	1987 Oct
PG 2304+042	23 07 02.66	+04 32 55.3	0.042	1987 Oct 27	MMT/BB	3200–6400	6	2400	...

NOTE.—Units of right ascension are hours, minutes, and seconds, and units of declination are degrees, arcminutes, and arcseconds.

[a] MMT: Multiple Mirror Telescope; FGS: Faint Object Grism CCD Spectrograph; BB: Big Blue Reticon; RC: Red channel, CCD spectrograph; CTIO: 1.5 m plus CCD spectrograph.

[b] Date (month) of spectrophotometry used to flux calibrate this spectrum.

[c] Data already published, McDowell et al. (1995).

[d] Redshift revised based on our spectra.

[e] Radio–X-ray SED in Elvis et al. (1994).

combining data sets from different measuring techniques and different authors. The EWs of optical and UV lines are listed in Tables 2 and 3, the UV and optical line fluxes in Tables 4 and 5, and the UV and optical FWHM in Tables 6 and 7. All values are in the rest frame.

2.3. *Spectral Energy Distributions*

The SEDs for the 11 quasars not presented in E94 were compiled here from a combination of our own ground-based optical and near-IR photometry (from the 0.6 m Fred Lawrence Whipple Observatory telescope, the MMT, the Mount Lemmon 61″ telescope, and the IRTF; for details see Table 8 and E94), as well as from the *Einstein* X-ray data, archival *IUE* or *HST* UV data, and *IRAS* far-IR data. The various data sets were combined following the method described in E94. When no optical photometry was available the MMT spectrophotometry was used. For inclusion in the SEDs, prominent emission lines were subtracted from the optical and UV spectrum and the spectrum binned into broader wavelength bands. A correction for Galactic extinction was applied to the SEDs based on the Galactic neutral hydrogen column and assuming a fixed conversion of $N(\mathrm{H\ I})/E(B-V) = 5.0 \times 10^{21}$ cm^2 mag^{-1} (Burstein & Heiles 1978). The Galactic H I column has been accurately measured by Elvis et al. (1986) for seven of the 11 objects. For the remaining four objects it was determined using the dereddening values from Neugebauer et al. (1987). After correcting for Galactic extinction, the data were blueshifted to the rest frame using a cosmological model with $\Omega_0 = 1$ and $H_0 = 50$ km s^{-1} Mpc^{-1}. No k-corrections and no assumptions about the intrinsic spectrum were required, since we were working with the complete SEDs. The contribution from the host galaxy was then subtracted using the method and template of E94 (based on the Sbc galaxy model of Coleman, Wu, & Weedman 1980) and normalized by the host galaxy monochromatic luminosity in the H band, which was taken from the literature or, when not available, set to $\frac{1}{3}$ of the luminosity of the quasar in that band (McLeod & Rieke 1994a, 1994b). The final SEDs for the 11 objects are displayed in Figure 3 in order of right ascension.

To allow comparison with earlier studies, in Table 9 we list several standard continuum parameters taken from the literature and determined in the usual way (i.e., not from the SEDs). These include: L_{opt} (luminosity at 2500 Å), L_{x} (X-ray luminosity at 2 keV), α_{ox} (effective optical–to–X-ray slope) from Wilkes et al. (1994), α_{x} (X-ray energy index, where $f_\nu \propto \nu^{-\alpha_{\mathrm{x}}}$) from Wilkes & Elvis (1987), α_{ouv} (optical slope, $f_\nu \propto \nu^{-\alpha_{\mathrm{ouv}}}$ taken between 1285 and 5100 Å) from Kuhn (1996), and radio class (quasar considered radio-loud [L] if $R_L > 1$, after E94). We also list the blue-bump strength measured from the SEDs, $C_{\mathrm{UV/IR}}$ (E94). In order to better characterize the SEDs, we directly measured the decade and octave luminosities, as defined in E94 (given in Tables 10

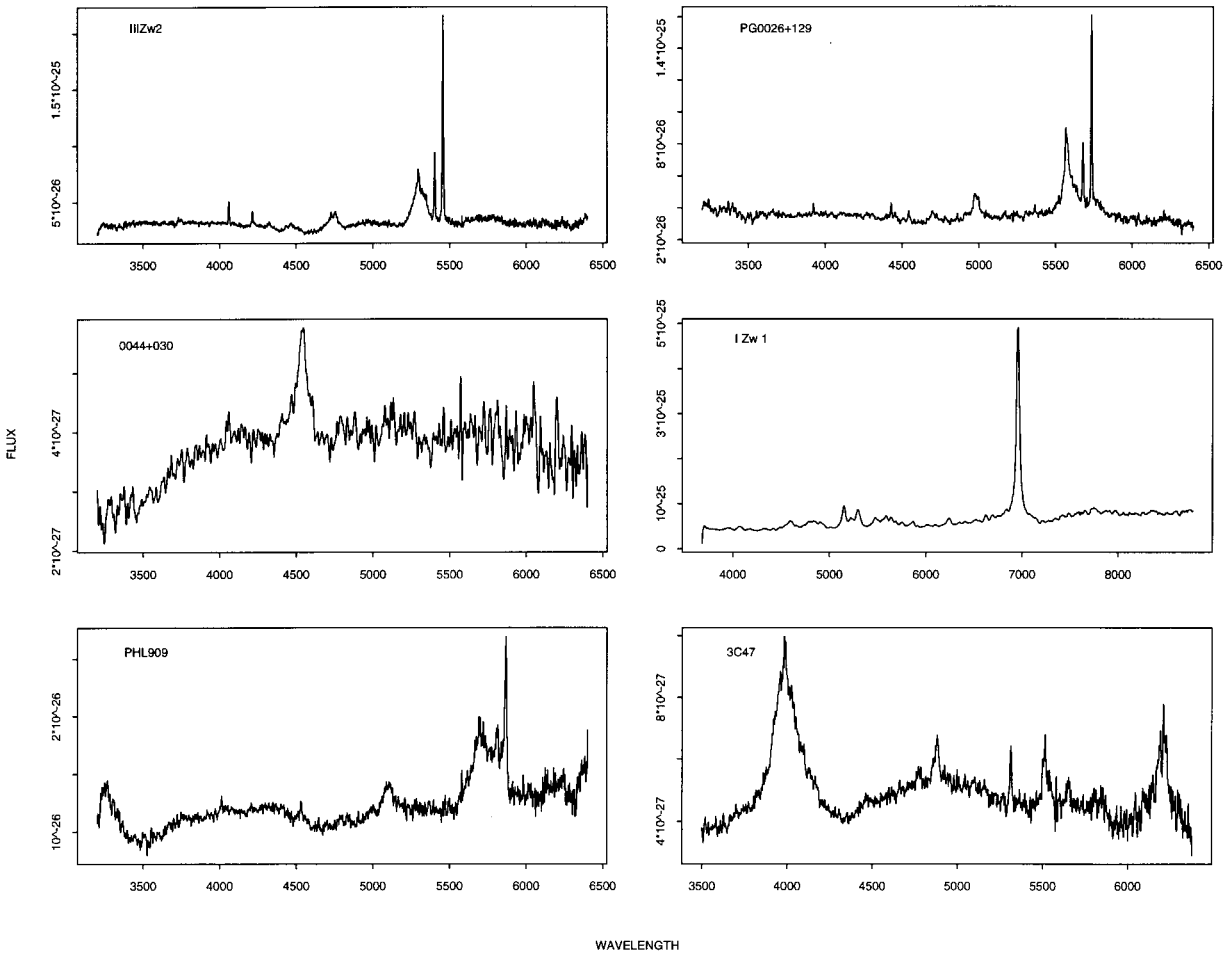

FIG. 2.—Optical spectrophotometry of the quasars in our sample in order of increasing right ascension and on a scale of F_ν (ergs cm^{-2} s^{-1} Hz^{-1}) as a function of λ (Å). Observational details are given in Table 1.

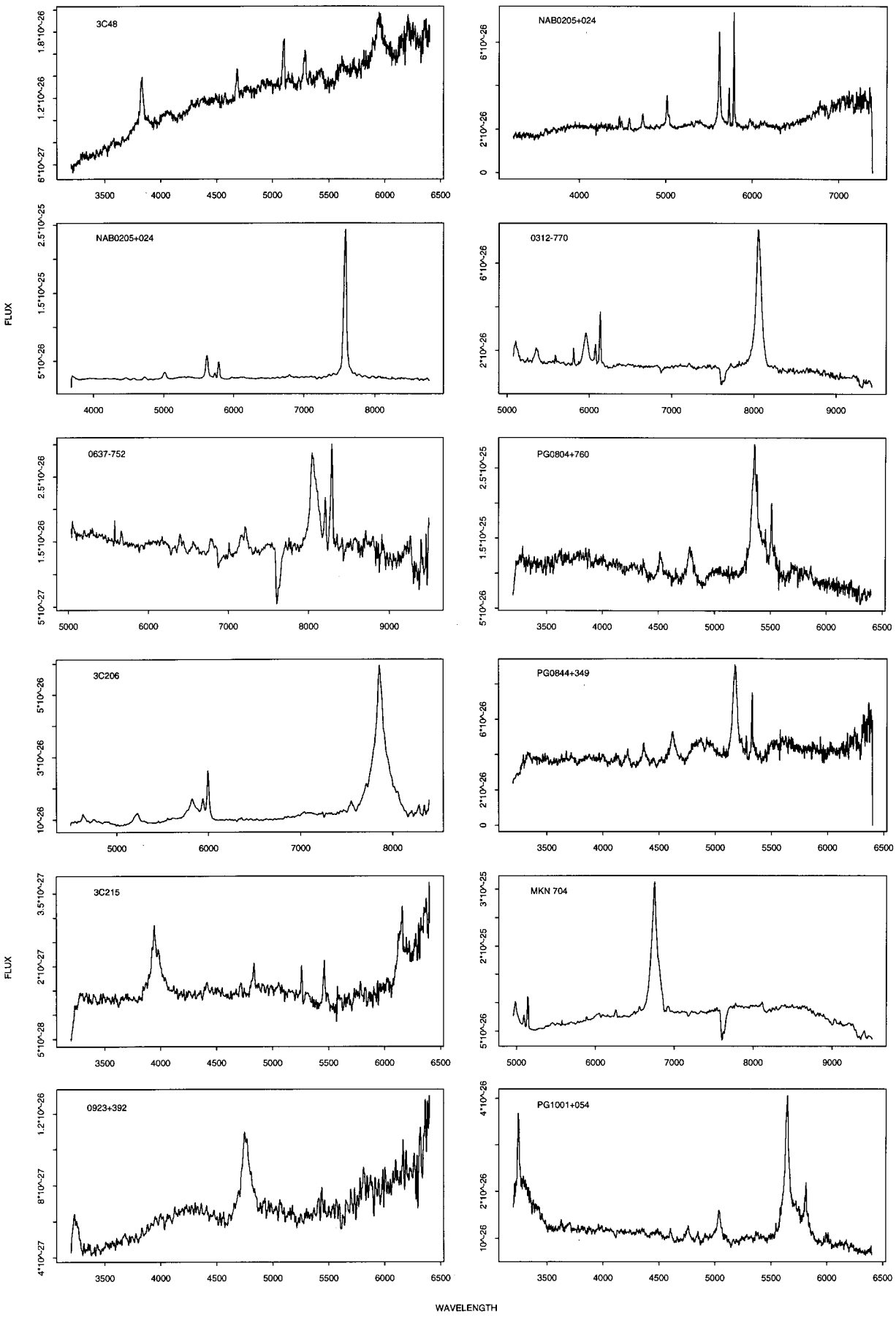

FIG. 2.—*Continued*

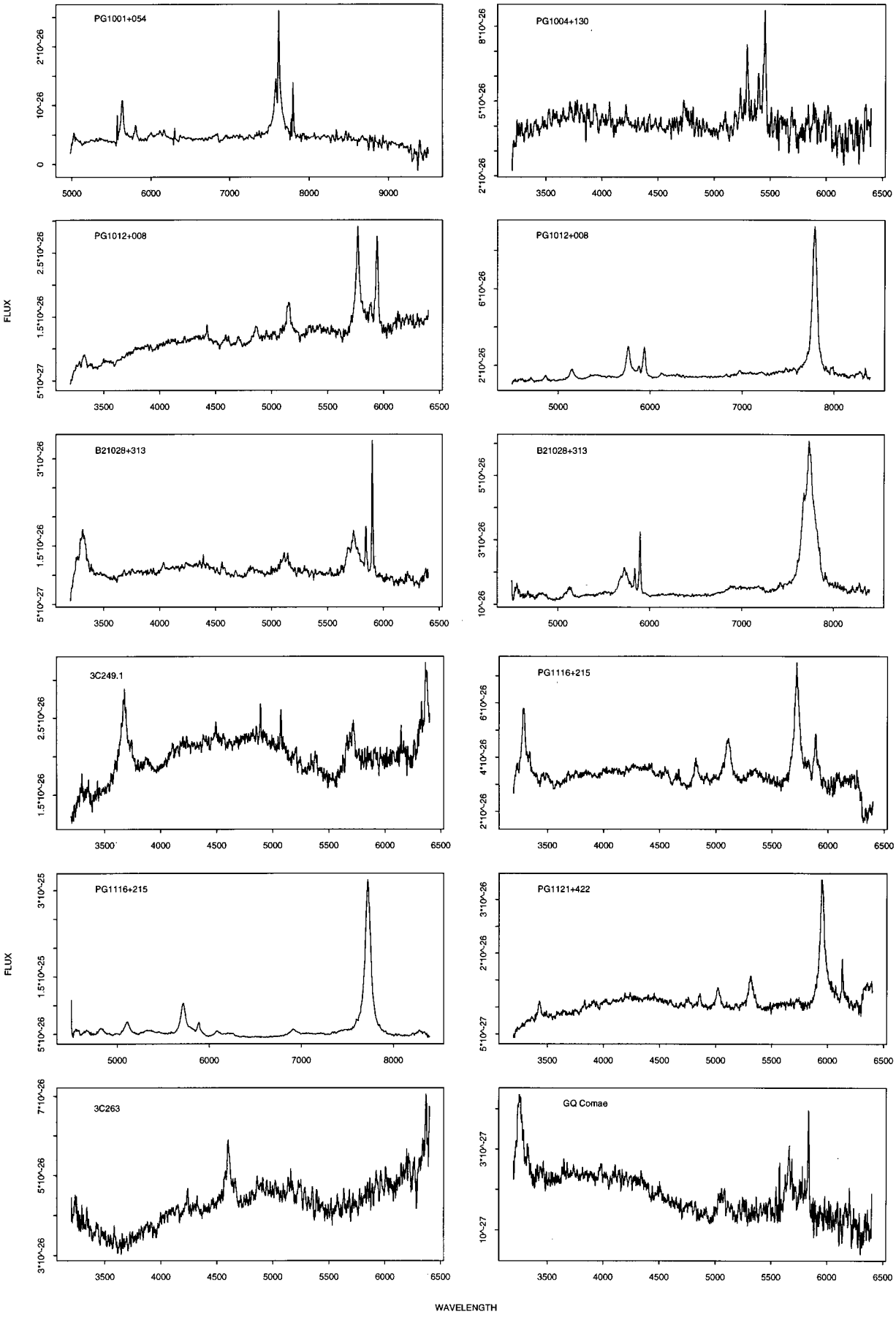

FIG. 2.—*Continued*

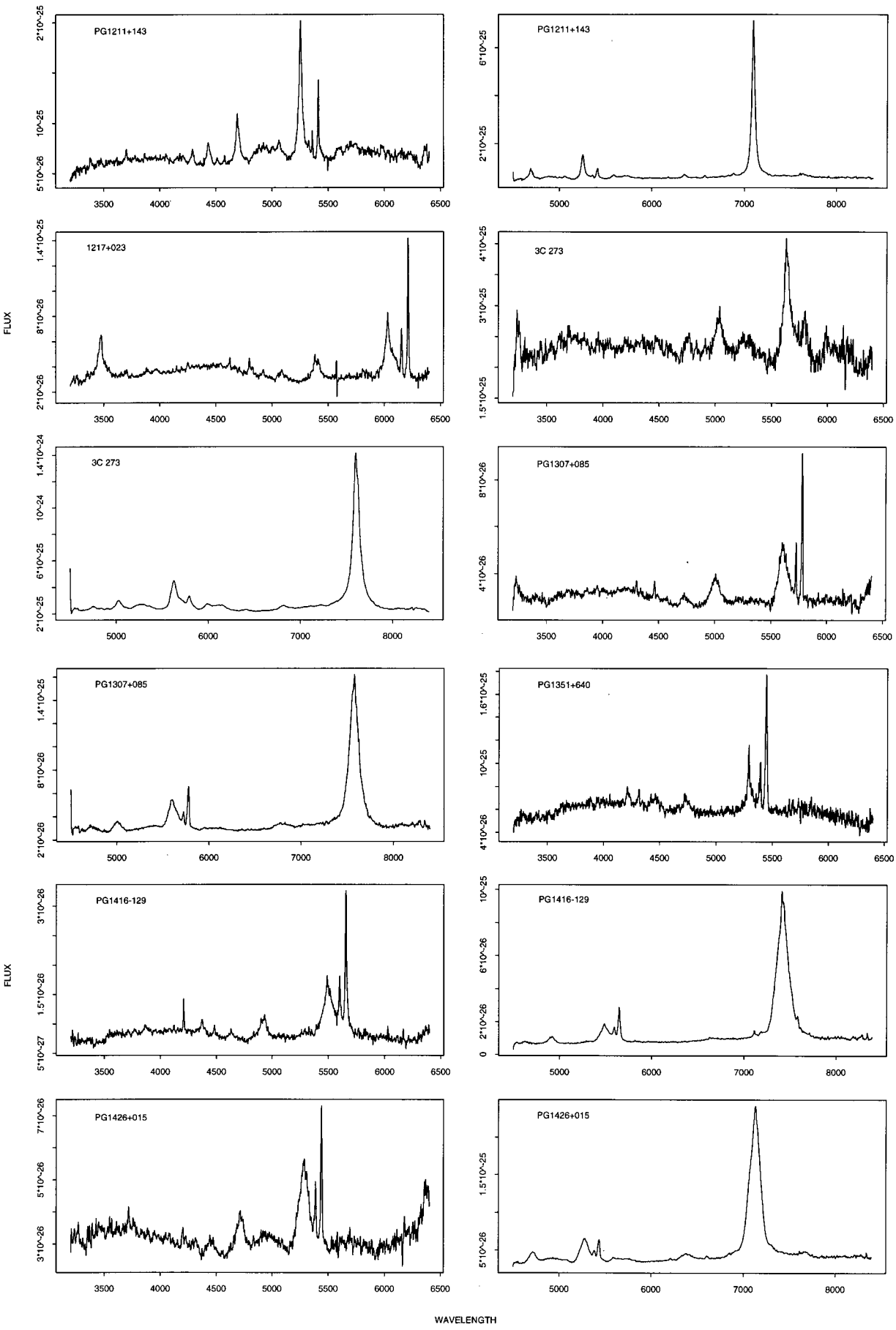

FIG. 2.—*Continued*

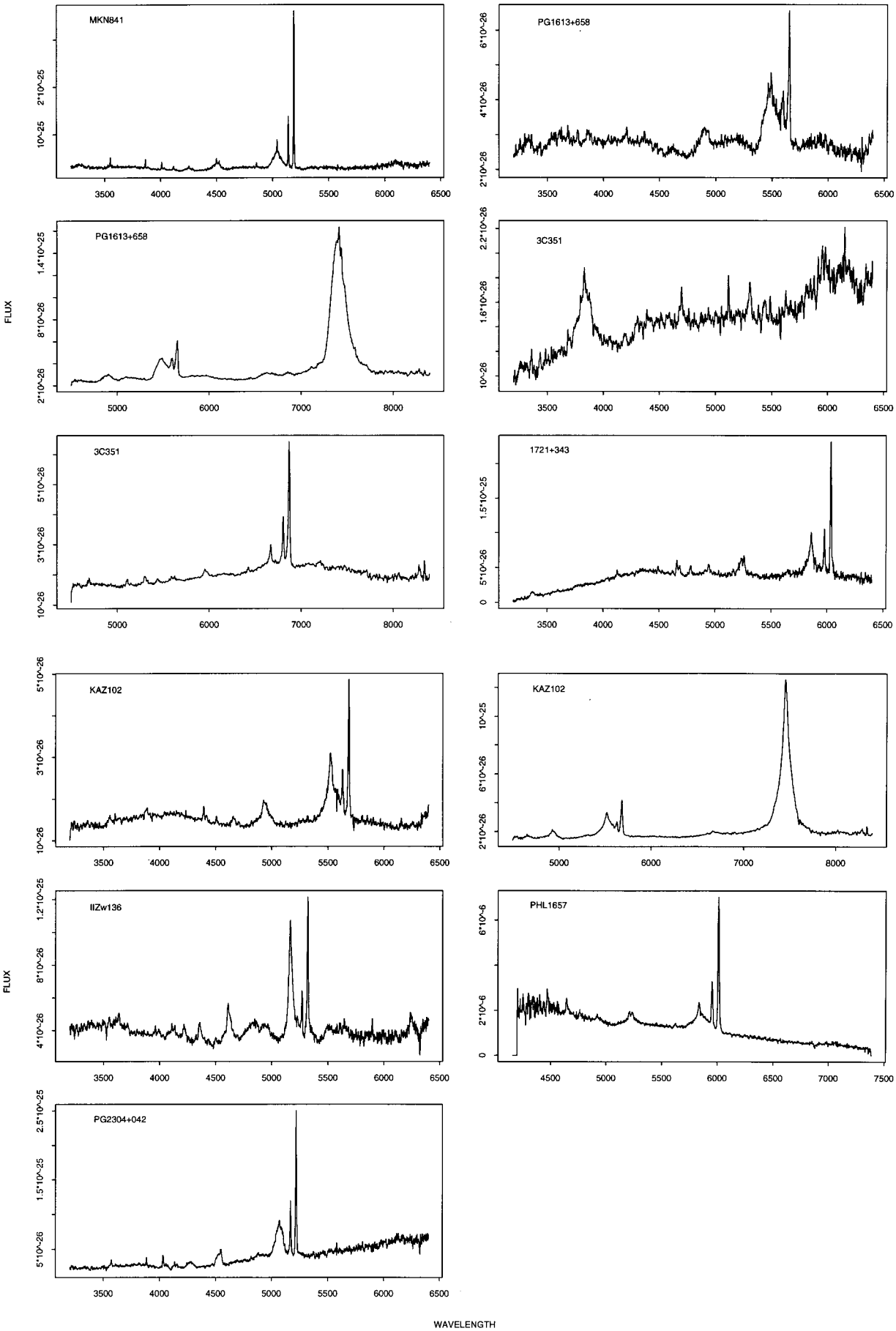

FIG. 2.—*Continued*

TABLE 2

UV-Line Rest Frame Equivalent Widths in Å

Name	Lyα N v λ1216	Lyβ O vi λ1034	C iv λ1549	Si iv O iv] λ1400	Al iii C iii] λ1909
0007+106.....	84.300	...	116.100	23.900	31.900
0026+129.....	64.300	...	34.700	<8.400	<29.000
0044+030.....	63.400	<15.000	50.800	50.300	27.900
0050+124.....	171.400	...	39.900	39.700	36.000
0054+145.....	87.400	...	112.600	<30.700	<79.000
0133+207.....	...	...	...	...	...
0134+329.....	<24.700	<14.700	<111.000	<16.800	<20.500
0205+024.....	60.900	...	38.500	<9.000	<38.700
0312−770.....	72.600	24.700	<83.100	<13.800	<285.200
0637−752.....	123.800	7.100	61.500	<121.500	<13.900
0804+761.....	101.800	...	81.700	28.000	63.700
0837−120.....	87.600	...	91.400	<16.500	<41.400
0844+349.....	113.600	...	18.500	27.900	<15.300
0903+169.....	...	...	...	...	...
0915+165.....	...	...	...	...	...
0923+392.....	...	...	...	...	...
1001+054.....	...	...	...	...	...
1004+130.....	9.100	<10.600	<66.500	<12.600	<77.700
1012+008.....	72.900	...	13.300	<13.500	...
1028+313.....	79.200	...	70.800	<12.100	<31.600
1100+772.....	57.800	7.700	90.800	<4.500	<19.800
1116+215.....	62.900	...	36.500	<4.100	31.200
1121+422.....	...	...	...	...	...
1137+661.....	75.300	13.100	44.800	46.700	<46.600
1202+281.....	74.200	...	129.100	<3.600	<46.600
1211+143.....	100.800	...	38.800	14.600	17.000
1217+023.....	138.200	28.300	173.000	38.900	<35.500
1226+023.....	46.100	...	36.600	4.800	10.000
1307+085.....	76.100	...	93.700	<15.100	<40.400
1351+640.....	70.900	...	30.300	25.500	25.400
1407+265.....	8.000	...	4.100	...	9.900
1416−129.....	134.100	...	181.800	<18.100	<292.700
1426+015.....	44.100	...	37.100	12.000	16.200
1501+106.....	...	...	...	...	...
1613+658.....	89.300	...	104.900	<6.600	33.300
1704+608.....	33.600	<3.600	49.800	<2.300	13.800
1721+343.....	126.300	30.200	94.000	<5.000	<23.900
1803+676.....	95.800	...	133.300	9.600	34.400
2130+099.....	110.400	...	56.600	23.300	18.200
2135−147.....	88.300	...	49.500	<6.800	<50.300
2304+042.....	...	...	...	...	...

and 11). In Table 12 we give several broadband luminosities: $L_{\rm UVOIR}$, $L_{\rm bol}$, $L_{\rm Lycon}$, and $L_{\rm Ion}$ (ionizing continuum), all defined as in E94. All SED parameters were measured using the TIGER software package written by J. McDowell (Wilkes & McDowell 1995). We have also measured the driving continuum for each line following Krolik & Kallman (1988; Table 2).

3. CORRELATION ANALYSIS

We studied correlations between the various line and continuum properties in Tables 13 and 14 using the ASURV statistical package (Isobe, Feigelson, & Nelson 1986), which includes allowance for the presence of upper limits in the sample. Specifically, we applied the following tests to each pair of parameters: the generalized Kendall rank test and the Spearman rank test, which is insensitive to outlying points. We considered a correlation real only if the probability of it occurring by chance was less than 2% in *both* of these tests. We present the percentage probability of a chance correlation in the generalized Kendall rank test followed by that for the Spearman rank test in Tables 13 and 14 for probabilities less than 5%. Significant correlations ($P < 2\%$) are in boldface type. When multiple correlations were found, we tested for the primary relation using ASURV bivariate Spearman ranks as input to partial Spearman rank analysis (Kendal & Stuart 1976). The primary correlations, i.e., the strongest pairwise correlations when the other variables are held constant, are italicized in Tables 13 and 14.

Since we are considering a large number of parameters (three parameters for each of 15 emission lines: EW, FWHM, flux, and 33 continuum parameters; see previous section), we divide our results up by emission-line parameters, first discussing the EW versus continuum luminosity correlations (§ 3.1), followed by the flux (§ 3.2) and the FWHM (§ 3.3). We then discuss the correlations between the various line parameters (§ 3.4) and between the various continuum parameters (§ 3.5). The number of correlations studied and found and the number of spurious correlations expected with $P < 2\%$ are shown in Table 15.

TABLE 3

OPTICAL-LINE REST FRAME EQUIVALENT WIDTHS (IN Å)

Name	Hβ λ4861	[O III] λ5007	Fe II λ4570	Hγ λ4340	Hδ λ4102	[Ne III] λ3968	[NeHe] λ3869	[O II] λ3727	[Ne V] λ3426	Mg II λ2798
0007+106.....	107.600	51.200	17.900	33.400	19.600	2.800	8.200	4.500	<2.600	...
0026+129.....	105.700	43.900	<6.600	24.700	11.400	<2.900	4.500	<1.600	<2.100	...
0044+030.....	...	...	...	...	...	...	<12.100	<7.700	<6.800	58.800
0050+124.....	80.500	19.000	70.400	18.900	<7.400	<6.700	<7.400	<2.100	...	...
0054+145.....	75.800	20.000	<6.600	12.200	<2.800	<3.200	<3.400	<1.200	<1.800	63.100
0133+207.....	...	...	...	...	21.200	<7.000	<4.000	<4.100	<8.200	205.300
0134+329.....	...	...	8.500	15.600	4.500	3.300	5.200	7.400	5.800	44.700
0205+024.....	52.600	26.800	14.100	20.900	7.600	4.600	5.200	<2.300	<1.800	...
0312−770.....	<55.600	7.700	24.800	<27.800	...	...	...	...	...	...
0637−752.....	63.700	17.600	<11.500	<19.700	<7.500	<8.300	<8.600	<2.300	<4.100	...
0804+761.....	123.200	24.800	17.700	29.100	11.500	4.700	5.100	<2.500	<3.300	...
0837−120.....	83.000	56.100	<7.300	20.600	<5.600	<4.200	8.800	...	...	...
0844+349.....	60.600	16.300	38.200	25.200	10.500	5.600	3.300	<1.800	<2.700	...
0903+169.....	...	...	...	31.700	<11.200	<6.500	9.900	7.400	7.400	108.300
0915+165.....	...	27.000	...	...	...	...	...	...	...	...
0923+392.....	...	...	...	...	...	...	...	<5.200	<7.900	60.800
1001+054.....	100.000	19.900	20.500	32.400	8.500	4.200	2.600	<1.600	2.600	...
1004+130.....	<17.700	<17.600	<30.400	<31.700	<8.400	<10.100	<9.600	<5.100	<5.600	<11.400
1012+008.....	63.200	26.400	15.400	22.800	7.700	<3.200	<3.400	2.400	<2.000	9.600
1028+313.....	87.700	26.000	<7.500	18.300	7.600	6.300	19.100	<1.600	2.900	77.900
1100+772.....	...	...	<7.200	19.600	5.500	<2.400	3.500	2.100	<1.900	62.100
1116+215.....	75.200	25.300	12.200	26.700	11.200	8.100	13.200	<1.300	<1.700	77.900
1121+422.....	118.500	11.400	10.800	29.200	13.300	5.400	3.700	<1.700	<1.500	25.000
1137+661.....	...	...	...	...	...	...	...	<2.700	<3.200	13.300
1202+281.....	74.600	24.500	<26.800	30.900	<15.400	<7.800	<7.400	<4.500	<5.500	45.200
1211+143.....	84.200	16.900	30.500	33.600	17.200	7.500	3.000	<1.500	3.300	...
1217+023.....	84.500	41.900	<9.000	30.500	9.400	<4.300	6.000	<2.000	<2.400	54.700
1226+023.....	69.400	11.800	17.500	15.500	5.100	2.900	<3.400	<2.100	<2.100	...
1307+085.....	72.200	24.200	4.600	38.100	11.300	5.400	3.900	<1.500	<1.700	...
1351+640.....	34.400	32.600	<8.300	14.000	8.900	3.600	4.900	<2.500	<2.700	...
1407+265.....	<40.000	...	...	...	...	...	...	...	...	20.700
1416−129.....	100.800	48.600	<5.800	33.800	5.600	<4.000	6.600	5.500	3.600	...
1426+015.....	85.900	30.000	12.100	25.400	18.100	3.500	4.800	<2.000	<3.500	...
1501+106.....	110.400	83.300	17.000	40.300	14.400	<3.700	6.000	3.700	7.800	...
1613+658.....	80.800	26.400	9.200	17.900	3.900	<2.300	3.900	1.900	3.700	...
1704+608.....	18.200	30.100	<2.800	6.100	3.500	<2.000	3.500	<2.300	3.100	30.400
1721+343.....	71.400	55.300	<10.500	33.500	9.900	<3.400	4.700	<2.200	3.900	47.600
1803+676.....	74.900	29.300	<5.100	39.200	4.600	<1.900	3.100	<1.500	3.100	...
2130+099.....	82.300	42.200	39.900	27.600	11.700	7.700	8.200	<1.800	3.900	...
2135−147.....	74.100	71.500	<2.500	20.100	3.000	<5.400	<5.400	<5.300	...	...
2304+042.....	83.400	48.900	<6.100	35.400	17.300	8.700	11.700	3.800	5.900	...

TABLE 4

UV Line Fluxes[a]

Name	log F(Lyα N v)	log F(Lyβ O vi)	log F(C iv)	log F(Si iv O iv])	log F(Al iii C iii])
0007+106.....	−11.583	...	−11.652	−12.296	−12.362
0026+129.....	−11.619	...	−12.069	< −12.613	< −12.166
0044+030.....	−11.499	< −12.224	−11.695	−11.749	−12.074
0050+124.....	−11.369	...	−12.077	−12.123	−12.144
0054+145.....	−11.989	...	−12.124	< −12.636	< −12.332
0133+207.....	...	...	...	...	...
0134+329.....	< −12.434	< −12.787	< −12.132	< −12.842	< −12.889
0205+024.....	−11.780	...	−12.168	< −12.732	< −12.099
0312−770.....	−11.650	−12.088	< −11.825	< −12.469	< −11.209
0637−752.....	−11.167	−12.318	−11.564	< −11.455	< −12.158
0804+761.....	−11.055	...	−11.378	−11.793	−11.477
0837−120.....	−11.748	...	−11.867	< −12.603	< −12.231
0844+349.....	−11.521	...	−12.364	−12.192	< −12.565
0903+169.....	...	...	...	...	...
0915+165.....	...	...	...	...	...
0923+392.....	...	...	...	...	...
1001+054.....	...	...	...	...	...
1004+130.....	−12.690	< −12.808	< −12.102	< −12.705	< −11.814
1012+008.....	−12.082	...	−12.916	< −12.896	-
1028+313.....	−11.807	...	−12.014	< −12.727	< −12.248
1100+772.....	−11.647	−12.520	−11.691	< −12.919	< −12.418
1116+215.....	−11.201	...	−11.593	< −12.501	−11.734
1121+422.....	...	...	...	...	...
1137+661.....	−11.533	−12.279	−11.910	−11.867	< −11.871
1202+281.....	−11.949	...	−11.934	< −13.385	< −12.313
1211+143.....	−11.256	...	−11.778	−12.170	−12.265
1217+023.....	−11.741	−12.470	−11.910	−12.506	< −12.663
1226+023.....	−10.807	...	−11.103	−11.921	−11.789
1307+085.....	−11.519	...	−11.696	< −12.404	< −12.100
1351+640.....	−11.677	...	−12.196	−12.269	−12.318
1407+265.....	...	...	...	...	
1416−129.....	−11.648	...	−11.683	< −12.619	< −11.958
1426+015.....	−11.249	...	−11.573	−12.013	−12.108
1501+106.....	...	...	...	...	...
1613+658.....	−11.653	...	−11.789	< −12.896	−12.344
1704+608.....	−12.019	< −13.018	−12.085	< −13.360	−12.715
1721+343.....	−11.265	−11.888	−11.518	< −12.764	< −12.314
1803+676.....	−11.483	...	−11.603	−12.679	−12.258
2130+099.....	−11.303	...	−11.729	−12.100	−12.373
2135−147.....	−11.935	...	−12.233	< −13.145	< −12.295
2304+042.....	...	...	...	...	...

[a] The fluxes are in ergs cm^{-2} s^{-1}.

3.1. *Equivalent Width–Continuum Luminosity Correlations*

3.1.1. *UV Lines*

The best known line-continuum correlation for quasars is the inverse correlation between the emission-line EWs and the continuum, commonly known as the Baldwin effect. It was detected for the first time by Baldwin (1977) in a sample of high-redshift quasars in which the EW of the C iv λ1549 line decreased with increasing UV continuum luminosity, L(1450 Å). The Baldwin effect has since been reported for a large number of lines (O vi, N v, He ii, C iii], Mg ii, and Lyα) in a number of different samples (e.g., Tytler & Fan 1992; Zamorani et al. 1992; Green 1996). Baldwin et al. (1978) showed, however, that the correlation is much stronger in a sample of flat-spectrum RLQs. This was later confirmed by Wampler et al. (1984) and Baldwin, Wampler, & Gaskell (1989). On the other hand, the analysis of optically selected quasar samples (Osmer 1980; Crampton, Cowley, & Hartwick 1990; Boyle, Jones, & Shanks 1991) shows that the Baldwin effect is less pronounced. It has been suggested that there exist two kinds of the Baldwin effect: a global, or object-to-object, effect and an intrinsic effect due to variability of the object (Pogge & Peterson 1992; Murdoch 1983). The slope of the intrinsic effect is different from that of the global one, adding scatter to the global relationship. However, as the result of variability and selection effects, some regions of the EW-L diagram may be left unpopulated and hence result in a more pronounced Baldwin effect for the RLQs.

The correlation results between EW and continuum luminosity are presented in Table 13, with coding explained in § 3. The primary correlations are italicized and are displayed for the Lyα, Hβ, and C iii] lines in Figures 4*a*, 4*b*, and 4*c*.

The Baldwin effect is present in our sample for the Lyα line, for which the EW anticorrelates with all the various optical and UV (OUV) luminosities. The primary correlation is with L(0.1–0.2 μm) luminosity.

The EW(C iii]) shows a very strong (primary) correlation

TABLE 5

OPTICAL LINE FLUXES[a]

Name	log F(Hβ)	log F([O III])	log F(Fe II)	log F(Hγ)	log F(Hδ)	log F([O II])	log F(Mg II)
0007+106.....	−12.338	−12.660	−13.088	−12.813	−13.020	−13.477	...
0026+129.....	−12.223	−12.605	<−13.413	−12.821	−13.131	<−13.852	...
0044+030.....	...	...	...	...	...	<−14.000	−12.843
0050+124.....	−12.267	−12.894	−12.327	−12.812	<−13.219	<−13.677	...
0054+145.....	−12.849	−13.428	<−13.860	−13.570	<−14.200	<−14.435	−12.643
0133+207.....	...	...	...	...	13.680	<−14.254	−12.256
0134+329.....	...	...	13.553	−13.277	−13.810	−13.560	−12.685
0205+024.....	−12.793	−13.085	−13.307	−13.097	−13.496	<−13.918	...
0312−770.....	<−12.890	−13.749	−13.237	<−13.066	...	...	...
0637−752.....	−12.714	−13.272	<−13.405	<−13.145	<−13.514	<−13.901	...
0804+761.....	−11.750	−12.446	−12.588	−12.334	−12.664	<−13.166	...
0837−120.....	−12.907	−13.077	<−13.903	−13.454	<−13.973	...	...
0844+349.....	−12.513	−13.083	−12.647	−12.809	−13.156	<−13.798	...
0903+169.....	...	...	...	−13.852	<−14.417	−14.845	−13.098
0915+165.....	...	...	...	...	...	...	...
0923+392.....	...	...	...	...	...	<−13.682	−12.609
1001+054.....	−12.588	−13.432	−13.749	−13.244	−13.763	<−14.337	...
1004+130.....	<−13.000	<−13.003	<−12.650	−12.570	<−13.116	<−13.256	<−12.656
1012+008.....	−12.927	−13.324	−13.472	−13.288	−13.713	−14.148	−13.527
1028+313.....	−12.904	−13.406	<−13.855	−13.440	−13.711	<−14.321	−12.551
1100+772.....	...	...	<−13.572	−13.122	−13.637	−14.048	−12.280
1116+215.....	−12.478	−12.951	−13.081	−12.796	−13.140	<−13.920	−12.050
1121+422.....	−12.720	−13.736	−13.719	−13.247	−13.534	<−14.302	−13.074
1137+661.....	...	...	...	...	...	<−13.316	−12.441
1202+281.....	−13.828	−14.312	<−14.182	−14.107	<−14.332	<−14.615	−13.420
1211+143.....	−12.217	−12.884	−12.556	−12.521	−12.697	<−13.639	...
1217+023.....	−12.408	−12.713	<−13.284	−12.733	−13.202	<−13.670	−12.100
1226+023.....	−11.609	−12.378	−12.236	−12.160	−12.532	<−12.898	...
1307+085.....	−12.542	−12.992	−13.641	−12.710	−13.328	<−13.914	...
1351+640.....	−12.573	−12.596	<−13.119	−12.845	−12.969	<−13.414	...
1407+265.....	...	...	...	...	...	...	...
1416−129.....	...	−13.236	<−14.148	−13.318	...	...	...
1426+015.....	−12.480	−12.937	−13.117	−12.807	−13.019	<−13.824	...
1501+106.....	−12.397	−12.519	−13.139	−12.758	−13.189	−13.599	...
1613+658.....	−12.515	−13.008	−13.404	−13.075	−13.715	−13.881	...
1704+608.....	−13.171	−12.953	<−13.944	−13.593	−13.812	<−13.997	−12.694
1721+343.....	−12.393	−12.504	<−13.128	−12.591	−13.057	<−13.596	−12.801
1803+676.....	−12.824	−13.211	<−13.912	−13.003	−13.888	<−14.229	...
2130+099.....	−12.390	−12.888	−12.659	−12.793	−13.130	<−13.796	...
2135−147.....	−12.950	−12.966	<−14.225	−13.258	−13.995	<−13.528	...
2304+042.....	−12.347	−12.579	<−13.504	−12.795	−13.107	−13.645	...

[a] The fluxes are in ergs cm^{-2} s^{-1}.

with L(1–2 keV) and a marginal correlation with L(0.1–0.2 μm). A C III]–X-ray correlation was reported by Green (1996) in a sample of quasars observed by the *Einstein* and *IUE* satellites. However, our C III] line sample has more than 50% upper limits, the correlation looks unconvincing (Fig. 4*b*), and no related correlation between the C III] flux and X-ray flux is seen (§ 3.2). This suggests that the EW(C III]) versus L(1–2 keV) correlation is spurious, and we cannot confirm the correlation reported by Green (1996).

The traditional Baldwin effect for the C IV line is not present in our sample (Fig. 5*a*). However, a significant correlation ($P < 1\%$ in all cases) is found for both C IV and C III] lines if we omit seven objects with low log νL_ν(0.1–0.2 μ), i.e., I Zw 1, NAB 0205+024, PG 0844+349, PG 1012+008, PG 1211+143, PG 1351+640, and II Zw 136. These objects have relatively weak carbon lines [EW(C IV)/EW(Lyα) < 0.55], as can be seen in Figures 5*a*, 5*b*, and 5*c*, where they are indicated by filled circles. They also have narrow FWHM of Hβ (less than 2500 km s^{-1}; Table 7) falling into the range of narrow-line Seyfert 1 (Sy1) objects (NLSy1; Osterbrock & Pogge 1985; except for PG 0844+349 and PG 1351+640, which are broad absorption line QSOs). This suggests that NLSy1s may have a systematically lower carbon-line EW and so do not follow the general Baldwin effect for the rest of the sample.

The only significant correlation involving α_{ox} is a strong anticorrelation with EW(C IV) (Fig. 6*a*). A marginal correlation with EW(Hβ) becomes significant when one object, PG 1001+054, is omitted (Table 13). For the O VI line, marginal anticorrelations of EW(O VI) with L_{opt} ($P_K = 1.7\%$, $P_S = 3.8\%$), and with α_{ox} ($P_K = 3.1\%$, $P_S = 4.1\%$) are present in our sample. The latter correlation was reported by Zheng, Kriss, & Davidsen (1995) in their sample of 30 QSOs and two Sy1s ($z > 0.15$), which had both *IUE* and *Einstein* X-ray fluxes. However, with only 10 points in our sample, we cannot draw strong conclusions from our lack of a correlation here.

TABLE 6

REST FRAME UV LINE WIDTHS[a]

NAME	FWHM				
	Lyα N V	Lyβ O VI	C IV	Si IV O IV]	Al III C III]
0007+106.....	3777.78	...	3660.42	8756.05	<3665.08
0026+129.....	1975.31	...	2734.66	4680.60	...
0044+030.....	10764.71	4467.18	5364.74	...	4496.84
0050+124.....	2629.63	...	5581.07	5337.08	<11324.01
0054+145.....	11780.27	...	7669.45	...	...
0133+207.....	...	...	...	...	...
0134+329.....	<7550.88	<3572.99	<4469.97	...	<2827.03
0205+024.....	1627.16	...	2519.69	<4498.93	<5942.90
0312−770.....	3074.08	6935.13	4491.28	...	...
0637−752.....	2985.19	6592.44	2829.56	...	<2985.36
0804+761.....	4498.77	...	4038.08	4810.31	11507.97
0837−120.....	5572.85	...	3960.61	...	...
0844+349.....	4054.33	...	4289.86	6719.19	<7603.27
0903+169.....	...	...	...	...	...
0915+165.....	...	...	...	...	...
0923+392.....	...	...	...	...	...
1001+054.....	...	...	...	...	...
1004+130.....	11884.96	...	...	<11703.44	...
1012+008.....	4822.23	...	5697.86	3100.93	...
1028+313.....	3454.33	...	3424.14	<4767.79	<4886.77
1100+772.....	3753.09	<7980.63	7772.10	<4171.66	<9246.97
1116+215.....	3241.98	...	6161.90	<5097.00	10209.39
1121+422.....	...	...	...	...	...
1137+661.....	4355.56	<7709.96	3710.77	<11596.07	3146.21
1202+281.....	4017.29	...	3780.50	3665.71	<5551.86
1211+143.....	2076.55	...	2733.50	7985.76	4436.14
1217+023.....	4037.04	3868.34	3788.24	5274.16	6245.26
1226+023.....	3634.57	...	4522.26	3708.66	4528.91
1307+085.....	3807.41	...	4545.51	5074.45	...
1351+640.....	2370.37	...	2112.97	7193.99	6025.60
1407+265.....	...	...	...	...	...
1416−129.....	5767.66	...	7355.70	<8199.00	...
1426+015.....	5234.58	...	4245.31	10146.32	5834.41
1501+106.....	...	...	...	...	...
1613+658.....	8203.47	...	8104.44	<6270.58	<8394.62
1704+608.....	6251.86	...	2424.79	<2235.08	4613.19
1721+343.....	3446.92	3818.97	4208.51	7342.17	<9141.15
1803+676.....	6637.54	...	3648.80	9098.79	<6982.36
2130+099.....	2133.34	...	2362.81	4464.57	3908.32
2135−147.....	7430.14	...	8140.08	<5499.43	<11830.29
2304+042.....	...	...	...	...	...

[a] FWHMs are in km s^{-1}.

3.1.2. *Balmer Lines*

The primary correlation for EW(Hβ) is with L(0.4–0.8 μm) (Fig. 4*c*). The EW(Hβ) also anticorrelates with the L(100–10 μm) IR luminosity, L(0.1–0.2 μm), OUV luminosities, and X-ray L(1–10 keV) luminosity (Table 13). A closer look shows that the "correlation" between EW(Hβ) and L(1–10 keV) is due to a systematically higher L(1–10 keV) for RLQs (Fig. 4*d*). The L(1–10 keV) luminosities are determined by extrapolating the *Einstein* soft X-ray (0.1–3.5 keV) flux and energy index. The systematically flatter α_x and stronger X-ray flux of the RLQs (Wilkes & Elvis 1987) exaggerates the systematic difference between L(1–10 keV) in the two classes.

Similar to Hβ, the EWs of the other Balmer lines anticorrelate with the far-IR luminosity, L(10–100 μm).

3.1.3. Fe II *Line*

No significant correlations are found for the EW of the Fe II λ4570 optical multiplet. The one with the lowest probability of chance occurrence ($P_K = 2.1\%$, $P_S = 3.5\%$) is an anticorrelation with L(1–2 keV) (reported as significant by Boroson & Green 1992 and others). However, Figure 7*a* does show a trend for objects with larger L(1–2 keV) luminosity and smaller EW (Fe II) to be RLQs, while radio-quiet objects have a much larger range in EW (Fe II) and concentrate toward smaller X-ray luminosities.

No correlation between the EW (Fe II) line and α_x is present in our sample (see Fig. 7*b*), nor in the RQQ and RLQ subsamples. Such correlations have been found by Wilkes, Elvis, & McHardy (1987) and Shastri et al. (1993) in samples observed by the *Einstein* satellite. However, Boroson (1989), studying a radio-selected sample, Walter & Fink (1993), who studied the Seyfert galaxies observed in the *ROSAT* All Sky Survey, and Zheng & O'Brien (1990) failed to confirm this correlation. Thirty-one objects in our sample are also included in the Shastri et al. (1993) sample;

TABLE 7

REST FRAME OPTICAL LINE WIDTHS[a]

NAME	FWHM								
	Hβ	[O III]	Hγ	Hδ	[Ne III]	NeHe	[O II]	Ne V	Mg II
0007+106.....	3840.59	527.92	3994.68	3712.33	2973.24	617.21	504.54	2300.36	...
0026+129.....	1518.21	395.45	2968.88	2847.15	459.68	471.44	...	507.88	...
0044+030.....	...	...	...	...	...	...	...	...	6374.92
0050+124.....	2589.60	<2193.52	6121.62	4304.73	4538.57	...	...	...	...
0054+145.....	4895.93	970.04	4087.99	1386.64	656.25	692.42	...	934.33	7447.43
0133+207.....	...	...	1216.58	1772.79	870.97	<1577.14	580.36	2758.33	12130.76
0134+329.....	...	...	3781.77	2695.76	2880.78	1635.30	1138.67	1162.53	4370.25
0205+024.....	1579.31	906.53	2554.13	1980.50	1940.02	932.79	...	...	...
0312−770.....	3185.16	813.66	2839.61	...	...	...	...	...	...
0637−752.....	3860.34	1011.56	4312.65	3800.09	4324.61	2119.92	...	1215.42	...
0804+761.....	3454.24	799.88	3465.19	2146.51	1305.70	...	429.84	<1598.96	...
0837−120.....	4038.08	1499.64	3944.49	3202.58	3247.23	<1645.38	...	...	...
0844+349.....	2555.54	534.45	3107.82	1951.24	2302.93	739.72	560.24	<534.15	...
0903+169.....	...	...	2006.67	3311.55	<2008.37	673.04	668.10	848.51	6905.65
0915+165.....	<2950.02	<1000.60	...	...	...	...	...	...	...
0923+392.....	...	...	...	...	...	...	...	...	5950.12
1001+054.....	2516.16	1026.96	1826.26	1932.23	1442.54	459.03	...	578.81	1475.33
1004+130.....	4728.06	1185.14	4188.64	<2932.71	...	...	...	...	...
1012+008.....	2112.54	1210.30	2732.47	2272.30	2311.24	517.96	590.83	<3679.44	3439.59
1028+313.....	5882.15	769.32	4717.71	4719.40	945.06	1052.98	410.52	1501.76	7347.18
1100+772.....	...	...	4622.32	1697.46	2801.92	690.87	445.13	1876.54	5528.21
1116+215.....	3086.42	1455.36	2771.87	3225.25	2639.37	<2231.57	...	...	3853.45
1121+422.....	2985.82	693.23	3732.07	2881.74	1787.30	<2677.42	...	1151.49	3593.98
1137+661.....	...	...	...	...	...	...	...	...	2864.89
1202+281.....	3306.13	517.08	4390.07	5752.07	<1179.44	<2341.68	...	...	6458.87
1211+143.....	1845.93	1118.03	2662.66	2594.83	1698.47	<2780.55	...	1435.21	...
1217+023.....	2123.65	624.32	4001.52	3768.65	<3411.52	655.98	...	855.52	3848.09
1226+023.....	4364.56	<2172.01	4150.20	3426.37	3325.11	...	...	3001.94	...
1307+085.....	5384.10	964.05	5030.15	4179.67	<2770.77	1017.31	599.68	<1352.46	<4290.90
1351+640.....	855.38	775.31	2056.44	4781.57	1517.39	<2692.15	587.61	...	...
1407+265.....	...	...	...	...	...	...	...	...	7611.48
1416−129.....	4360.24	1097.66	4105.27	1906.63	1054.69	1413.54	567.64	2551.24	...
1426+015.....	5835.25	1257.64	4677.62	5723.55	1601.31	1170.84	...	1023.65	...
1501+106.....	1865.67	418.21	4409.28	2477.08	719.76	593.95	436.28	686.52	...
1613+658.....	6997.36	1270.22	5177.39	3983.66	3720.52	606.35	1000.54	2990.99	...
1704+608.....	1209.02	977.83	3116.11	<2320.28	2269.66	2273.44	426.62	1811.04	7817.77
1721+343.....	2400.75	699.82	3787.72	1334.71	1010.08	968.46	668.10	639.23	3716.21
1803+676.....	2848.19	948.89	4054.81	1582.64	873.24	505.55	459.62	1884.42	...
2130+099.....	2058.85	608.15	2664.73	2138.47	2207.67	714.91	610.95	2621.03	...
2135−147.....	2511.84	827.50	4255.55	1191.37	1168.10	999.48	760.67	...	4185.83
2304+042.....	4093.01	620.73	3325.69	4333.25	1209.68	894.02	474.91	718.92	...

[a] FWHMs are in km s^{-1}.

however, only 16 of them have Fe II measurements. A comparison of our Figure 7*b* with their Figure 5*a* shows small disagreements between the measured values and one incorrect slope. PG 0844+349 has an X-ray energy index α_x of 1.6 in Shastri et al. (1993), whereas the correct value from the *Einstein* data is 0.6 (E94).

Given the apparently discrepant results in the literature, we conclude (as did Lawrence et al. 1997) that there is no direct correlation between Fe II and α_x, but rather a zone of avoidance such that objects with flat X-ray spectra do not have strong Fe II. A similar effect, that objects with stronger X-ray luminosities do not have strong Fe II, would also explain our marginal correlation between Fe II and L(1–2 keV) (Fig. 7*a*). This also agrees with the long-established tendency toward weak Fe II in RLQs (Peterson, Foltz, & Byard 1981; Phillips 1977; Osterbrock 1977).

Lawrence et al. (1997) note a much stronger correlation between Fe II and the near-IR–X-ray slope α_{ix}. We tested for this in our sample and found no significant correlation ($P_K = 5.0\%$, $P_S = 6.9\%$). However, our data cover only about 60% of the range in α_{ix} and a smaller range in log(Fe II/Hβ) than that of Lawrence et al. (1997; −1.5 to 0 in our sample; see −1 to 0.7 in theirs).

3.2. *Line Flux versus Continuum Flux Correlations*

The OUV line flux–continuum flux correlations are presented in Table 14, with similar coding to Table 13. This analysis was performed identically in both flux and luminosity space to guard against purely redshift-induced results. However, given the small range in redshift ($z < 0.4$ for all but five sources; Fig. 1), there is no significant difference between the two sets of results. All the primary correlations for these lines are shown in Figure 8. For Lyα and C IV lines the primary correlations are with the continuum regions closest to the driving continuum, as is expected. However, we note that simultaneous measurements of both

TABLE 8

SED Details for Objects Not Included in E94[a]

Name	Radio Data	Far-IR Data	Optical Data	UV Data	X-Ray Data	$E(B-V)$	Starlight log $\nu L_{\nu H}$	Starlight Reference
0044+030.....	1	12	15, 16	24[b]	26	0.06	$45.30^{+0.15}_{-0.15}$	31
0133+207.....	2, 3, 4, 5	13	17, 18	25	30	0.056	$45.10^{+0.15}_{-0.15}$	31
0903+169.....	4, 5, 6	13	15	25[c]	26, 27	0.076	$44.42^{+0.12}_{-0.12}$	32
0923+392.....	5, 6, 7, 8	14	15, 19	25[d]	27	0.032	$45.60^{+0.15}_{-0.15}$	31
1001+054.....	1, 9	14	15, 19, 20	...	26	0.04	$44.20^{+0.12}_{-0.12}$	34
1004+130.....	...	12, 13	16, 20, 21, 22, 23	24	26	0.07	$44.80^{+0.12}_{-0.12}$	33
1012+008.....	1	12	16, 17	24	...	0.065	$44.91^{+0.12}_{-0.12}$	33
1121+422.....	1	12	15, 16, 17	25	...	0.047	$44.65^{+0.12}_{-0.12}$	33
1217+023.....	7, 10	13	15, 17, 20, 23	24	27, 28, 29	0.039	$44.58^{+0.12}_{-0.12}$	35
1351+640.....	1, 11	14	16, 21	24	26	0.05	$44.38^{+0.11}_{-0.12}$	34
2304+042.....	1	13	15, 17	...	...	0.110	$43.66^{+0.15}_{-0.15}$	36

[a] Elvis et al. 1994.

[b] The UV spectrum was deleted, as the difference between optical and UV spectra was 0.5 in log νL_ν.

[c] UV grayshifted by -0.193 in νL_ν.

[d] UV grayshifted by -0.308 in νL_ν.

References.—Radio data: (1) Kellermann et al. 1989; (2) Bentley et al. 1975; (3) Swarup, Sinha, & Hilldrup 1984; (4) Pooley & Henbest 1974; (5) Steppe et al. 1988; (6) Owen et al. 1978; (7) Owen & Puschell 1982; (8) Parley 1982; (9) Condon et al. 1981; (10) Miley & Hartsuijker 1978; (11) Robson et al. 1985. Far-IR data: (12) Sanders et al. 1989; (13) E94; (14) Neugebauer et al. 1986. Optical and near-IR data: (15) this paper; (16) Neugebauer et al. 1987; (17) E94; (18) Penfold 1979; (19) Ennis & Neugebauer 1982; (20) Hyland & Allen 1982; (21) Neugebauer et al. 1979; (22) Sitko et al. 1982; (23) Cutri et al. 1985. UV data: (24) *IUE* data from Lanzetta, Turnshek, & Sandoval 1993; (25) *HST* data; A. Dobrzycki 1998, private communication. X-ray data: (26) Wilkes et al. 1994; (27) Wilkes & Elvis 1987; (28) Comastri et al. 1992; (29) Williams et al. 1992; (30) Wilkes et al. 1994. Starlight Reference: (31) $\frac{1}{3}$ total L; (32) Romanishin & Hintzen 1989; (33) McLeod & Rieke 1994a; (34) McLeod & Rieke 1994b; (35) Taylor et al. 1996; (36) Smith et al. 1986.

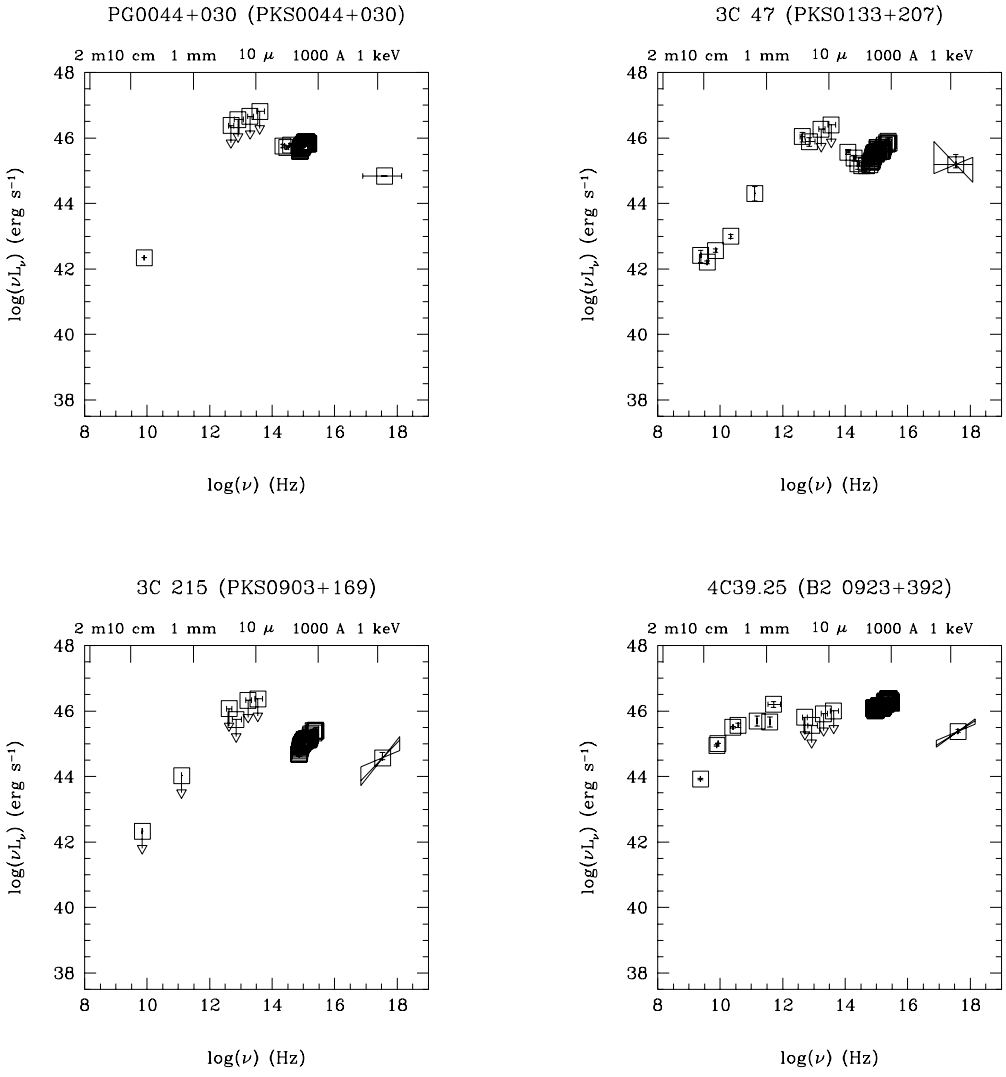

Fig. 3.—Radio–X-ray SEDs for the 11 new objects (Table 8) on a log νL_ν vs. log ν scale.

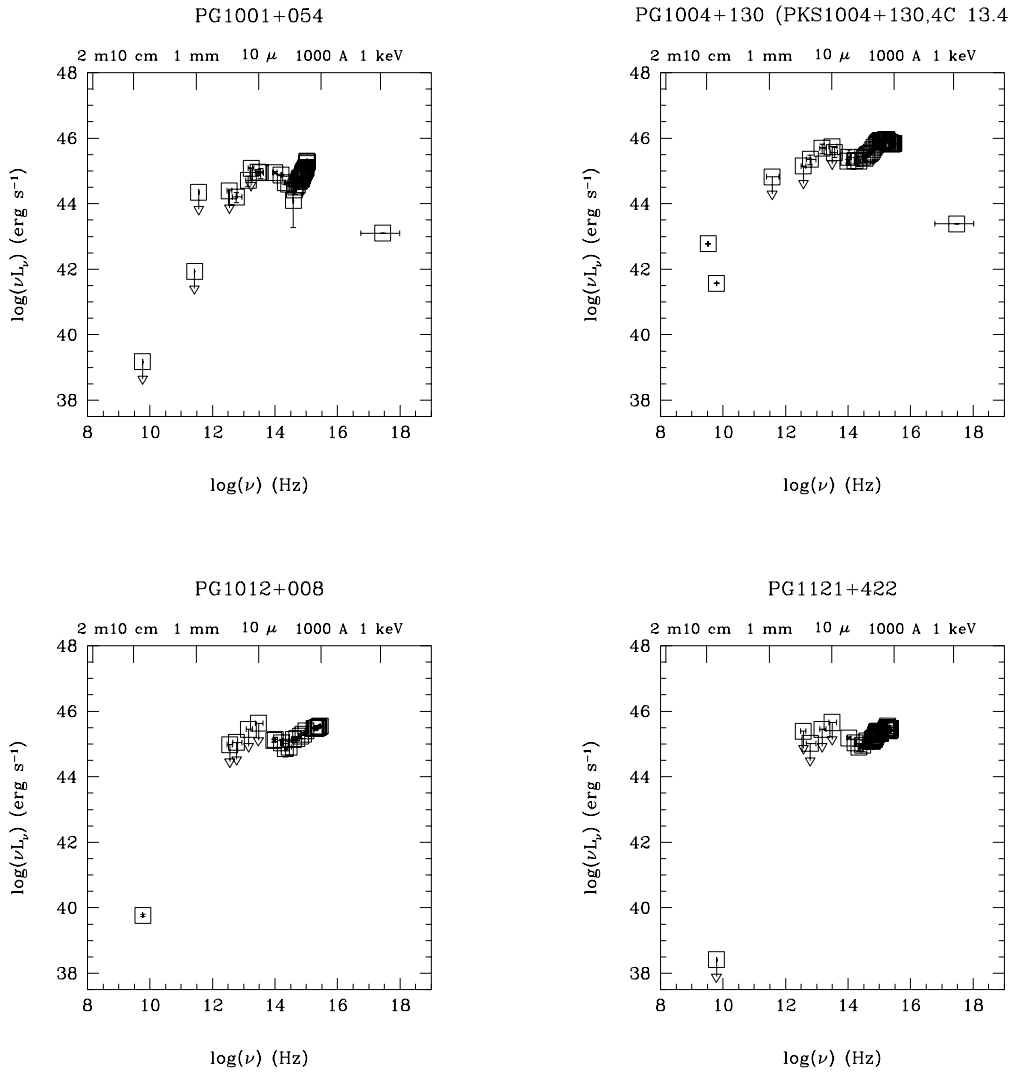

FIG. 3.—*Continued*

UV lines and continuum (as is the case in our sample) will result in smaller scatter and lower probabilities for these correlations. In other bands, small continuum variations or systematic shifts between the measurements will add scatter.

For the C III] line the primary correlation is with the optical flux, far from its driving continuum. No conclusions can be drawn for the Si IV line, as it is not clear what the driving continuum is for this line (T. Kallman 1997, private communication). Correlations for Lyα flux and EW are the most significant (usually $P \ll 0.1\%$; compare $P \gg 0.3\%$; see Table 14) and have the smallest scatter among the UV lines (Table 16). The predominance of the EW(Lyα) correlations reported in the previous section may be due to the primary correlation being with the local continuum for this line (Table 14). Thus the EW is determined by only two parameters, the line flux and the local continuum, whereas for lines whose primary correlation is not with the local continuum, nonsimultaneity and calibration uncertainties between the different continuum regions can induce additional scatter.

3.2.1. *Line Flux versus Driving Continuum Correlations*

We investigate the correlations between the strengths of the broad emission lines such as Lyα, O VI, C IV, C III], Balmer lines, Fe II, and their driving continua. To determine the driving continua, the SEDs were linearly interpolated between observational points in the OUV. In the X-rays the observed α_x was used, and the EUV continuum was determined by a linear interpolation between the lowest energy point in the X-ray range and the highest in the UV. Then the spectrum was integrated over the energy range of the driving (ionizing) continuum of each line (see Table 14) following the definitions of Krolik & Kallman (1988; see their Table 4). The probability of a correlation between each line and its driving continuum, as given by the Kendall and Spearman rank tests, is shown in Table 14. The slopes of the linear regression and the scatter of the observational points around the regression line are shown in Table 16. All correlations between the lines and driving continuum are shown in Figure 9. While these correlations are strong, surprisingly in no case were they the primary line versus continuum correlations. In addition, the slopes of the regression lines were always smaller than the expected value of 1. Possible explanations include differing line and continuum reddening, optically thin (matter bounded) clouds, and continuum emission from an accretion disk (see the discussion in § 4.1.3).

3.3. *Line FWHM versus Continuum Luminosity Correlations*

Only two significant correlations were found between optical/UV line widths and continuum luminosity param-

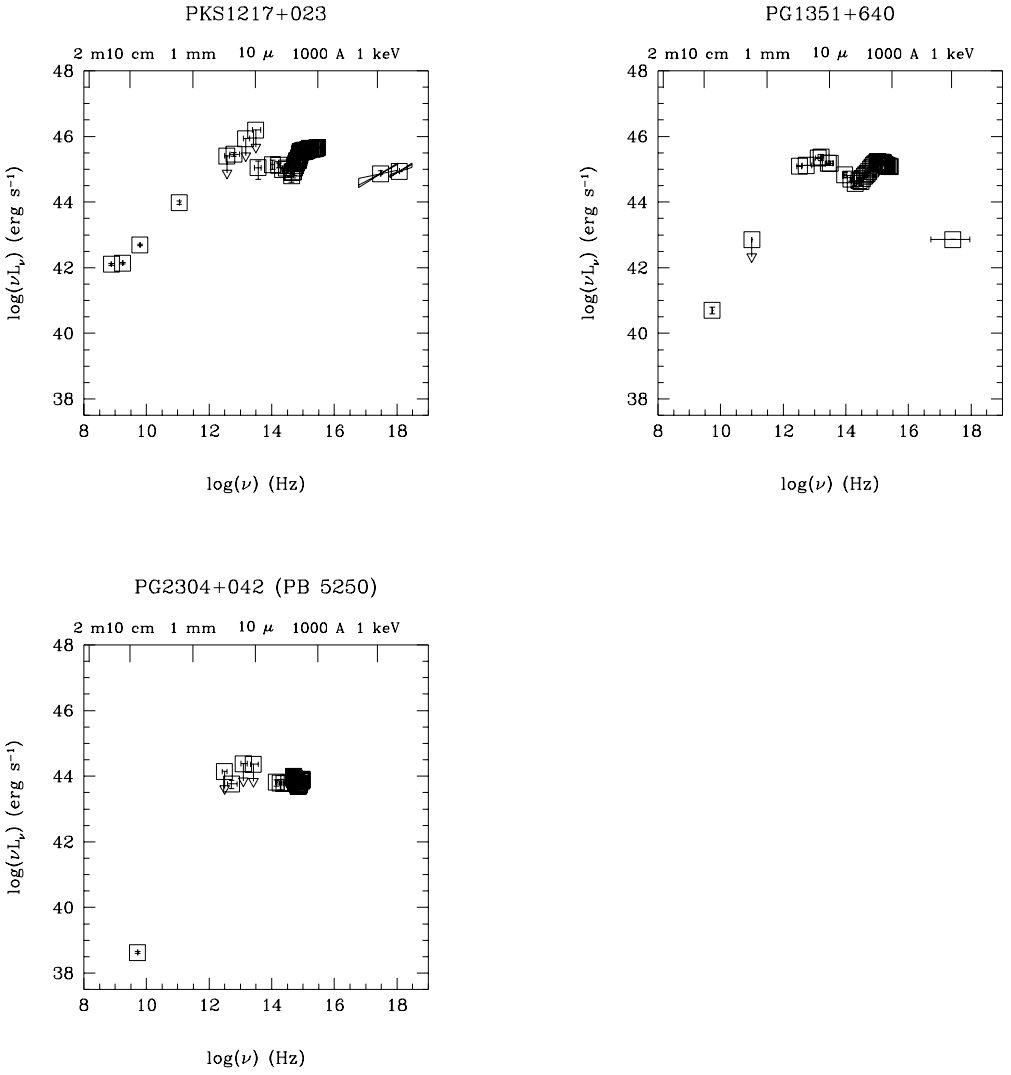

FIG. 3.—*Continued*

eters: FWHM(NeHe) with far-IR (10–100 μm) luminosity ($P_K = 1.9\%$, $P_S = 1.5\%$) and FWHM ([O III]) with $L_{\rm Ion}$ (1.3%, 1.3%). NeHe also correlates but less significantly with L(0.1–0.2 μm) (2.4, 2.7%) and $L_{\rm bol}$ (2.2%, 1.7%).

As has been noted in Table 15, the number of spurious correlations with a probability of a chance correlation less than 2% is expected to be six for the 315 correlations tested. Since we found fewer than six significant correlations, we consider it likely that they are spurious.

3.4. *Correlations vetween Emission-Line Parameters*

We have also studied correlations between the various parameters of each emission line. We shall present here only those correlations that are significant and/or interesting.

The EWs of the Balmer lines correlate with each other, and the FWHM(Hβ) correlates with FWHM(Hγ). This is consistent with photoionization models, as the Balmer lines are expected to form in the same region.

The Lyα and C IV line EW and FWHM also correlate with each other (Fig. 10). These correlations are easily understood in the light of standard photoionization models, as it is generally believed that these lines originate in clouds located at the same distance from the continuum source. However, the presence of a correlation, also reported by Corbin (1991) and Corbin & Boroson (1996), between the EW(Lyα), EW(C IV), and EW(Hβ), as well as FWHM(Lyα), FWHM(C IV), and FWHM(Hβ) (and also FWHM of Hγ), is interesting. Hβ (and Hγ) is a low-ionization line and is expected to form in a different region than the C IV and Lyα lines. If both the high- and low-ionization components scale similarly with luminosity, two models are applicable. First, the Collin-Souffrin et al. (1988) model, where low-ionization lines (LILs) are formed in the atmosphere of the accretion disk, while high-ionization lines (HILs) form in a distinct spherical component. Second, the standard model, where LILs and HILs are formed in the same cloud but in zones of differing ionization.

We see no correlations between the EW and FWHM of individual lines in our sample. An anticorrelation has been reported for C IV in some samples (e.g., Francis et al. 1992; Wills et al. 1993; Corbin & Francis 1994).

The EW([O III]) anticorrelates with EW(Fe II) (see Fig. 11). This relation was noted by Boroson & Green (1992) and dominates their first eigenvector. They rule out an interpretation based on the standard beaming model partly because of the strong dependence on [O III], which is

TABLE 9

CONTINUUM PARAMETERS

Name	α_{ox}	α_x	$C_{UV/IR}$	Radio Loud/Quiet	L_{opt} [a]	L_x	α_{ouv} [b]
III Zw 2.....	1.14	0.4	0.47	L	29.74	26.59	-0.30 ± 0.02
PG 0026+129.....	1.41	0.9	0.49	Q	30.58	26.92	-0.26 ± 0.03
0044+030	1.59	...	...	L	31.49	27.34	...
I Zw 1.....	1.42	1.7	...	Q	30.07	26.36	...
PHL 909.....	1.28	0.3	−0.08	Q	30.09	26.27	...
3C 47.....	1.01	0.9	0.00	L	30.34	27.71	...
3C 48.....	1.28	0.7	0.18	L	30.77	27.45	-0.61 ± 0.16
NAB 0205+024.....	1.33	1.2	0.56	L	30.33	26.87	-0.43 ± 0.06
PKS 0312−770	1.32	0.1	...	L	30.54	27.08	...
PKS 0637−752	1.29	0.5	...	L	31.67	28.35	...
PG 0804+760.....	1.28	0.0	0.60	Q	30.14	26.80	-0.36 ± 0.08
3C 206	1.24	0.7	0.49	L	30.59	27.36	0.51 ± 0.03
PG 0844+349.....	1.65	0.6	0.44	Q	30.21	25.93	-0.61 ± 0.04
3C 215	1.14	0.0	0.00	L	30.11	27.16	...
Mrk 704	1.35	0.3	...	Q	29.15	25.63	...
0923+392	1.12	0.4	0.64	L	30.82	27.97	...
PG 1001+054.....	>1.76	...	...	Q	30.16	<25.57	...
PG 1004+130.....	>1.84	...	...	Q	30.64	<25.86	...
PG 1012+008.....	...	...	0.25	Q	30.36	...	
B21028+103	1.11	0.5	0.46	L	29.87	27.00	-0.26 ± 0.04
3C 249.1	1.33	1.0	0.30	L	30.89	27.45	-0.45 ± 0.02
PG 1116+215.....	1.39	1.0	0.59	Q	30.63	27.02	-0.24 ± 0.05
PG 1121+422.....	...	...	...	Q	30.26	...	
3C 263	1.31	0.7	0.70	L	31.31	27.91	...
GQ Comae	1.38	1.1	0.25	Q	30.63	27.04	-0.70 ± 0.07
PG 1211+143.....	1.17	1.8	0.46	Q	30.19	27.16	-0.87 ± 0.04
PKS 1217+023	1.16	0.5	0.48	L	30.38	27.32	...
3C 273	1.30	0.3	0.32	L	31.46	28.07	...
PG 1307+085.....	1.43	0.9	0.61	Q	30.47	26.97	-0.40 ± 0.04
PG 1351+640.....	>1.76	...	...	Q	29.91	<25.32	...
PG 1407+265.....	1.44	1.2	0.64	Q	32.01	28.47	...
PG 1416−129.....	1.26	0.9	0.53	Q	30.39	26.93	-0.07 ± 0.05
PG 1426+015.....	1.36	0.9	0.69	Q	30.04	26.70	0.09 ± 0.03
Mrk 841	1.30	1.0	0.38	Q	29.24	26.32	...
PG 1613+658.....	1.32	1.1	0.28	Q	30.27	26.85	-0.28 ± 0.05
3C 351	1.60	0.1	0.40	L	31.02	26.86	...
1721+343	0.98	0.5	0.72	L	30.09	27.54	-0.10 ± 0.04
KAZ 102.....	1.41	−0.2	0.40	Q	30.11	26.44	-0.46 ± 0.04
II Zw 136.....	1.46	0.8	0.42	Q	29.96	26.32	-0.49 ± 0.06
PHL 1657	1.32	0.5	0.15	L	30.62	27.19	-0.78 ± 0.04
PG 2304+042.....	...	...	...	Q	...	...	

[a] L_{opt} is a standard definition of luminosity at 2500 Å obtained by extrapolating B (or V) magnitude and assuming a continuum slope of 0.5.

[b] Slope ($f_\nu \propto \nu^{-\alpha}$) between 1285 and 5100 Å, taken from Kuhn 1996.

thought to be isotropic and partly because of the positive correlation of absolute continuum magnitude with the magnitude of [O III], which is not expected if beaming causes the range in optical continuum flux. Instead, they favor a model based on a geometric effect intrinsic to the quasar, such as shadowing of the narrow-line region (NLR) by a coplanar, toroidal-shaped broad-line region (BLR) so that the covering factor, perhaps determined by the ratio of accretion rate to the Eddington rate, drives the correlations. Eddington-limited flow was also suggested to explain those objects with extremely strong Fe II emission (Pounds et al. 1996) based primarily on their unusually steep, soft X-ray spectra.

Since [O III] and [O II] originate in similar parts of the NLR, we expect their emission-line profiles to be similar. We find a correlation between their EWs, but we do not see a correlation for their FWHM. However, we do not place much weight on this latter result, as the narrow lines are often close to the spectral resolution, [O II] is weak, and we have only 19 measurements of variable quality.

3.5. *Continuum-Continuum Correlations*

All the continuum luminosities correlate with one another. The regression slopes for L_1 versus L_2 and L_2 versus L_1 relations are presented in Table 17. Most of the relations have regression slopes near unity. The exception is the L(0.1–0.2 μm) versus L(0.2–0.4 μm) relation, whose slope is less than 1, indicating that L(0.1–0.2 μm) increases faster with increasing bolometric luminosity than any other luminosity. This could be explained if the peak of the big blue bump (BBB) moves from the EUV into the UV as the luminosity increases.

Correlations with the spectral indices were also investigated. The only correlations found were those between L_x, L(1–2 keV), and α_{ox} (regression slope = -1.51 ± 0.83 and -1.88 ± 0.7, respectively), showing the steepening of α_{ox}

TABLE 10

DECADE LUMINOSITIES[a]

NAME	LUMINOSITY				
	10–100 μm	1–10 μm	0.1–1 μm	0.1–1 keV	1–10 keV
0007+106.....	45.110	45.240	45.410	44.300	44.970
0026+129.....	<45.020	45.390	45.720	44.790	44.920
0044+030.....	<46.910	45.880	46.110	...	...
0050+124.....	45.670	45.540	45.270	45.070	...
0054+145.....	45.660	45.630	45.590	44.240	44.820
0133+207.....	46.240	45.930	45.930	45.550	...
0134+329.....	46.610	46.040	46.020	45.090	...
0205+024.....	45.350	45.370	45.680	44.550	...
0312−770.....	<45.560	45.210	45.910	44.350	...
0637−752.....	46.770	46.820	47.030	45.880	46.240
0804+761.....	45.330	45.530	45.700	44.710	44.690
0837−120.....	45.200	45.400	45.640	45.060	45.220
0844+349.....	44.800	44.730	45.180	43.470	...
0903+169.....	<46.490	<46.430	45.550	44.680	...
0915+165.....	44.620	44.640	44.160	43.120	...
0923+392.....	<46.170	<46.540	46.540	45.340	45.750
1001+054.....	44.960	45.340	45.330	...	...
1004+130.....	45.860	45.780	46.200	...	...
1012+008.....	<45.690	45.290	45.560	...	...
1028+313.....	<45.640	45.160	45.520	44.520	44.970
1100+772.....	45.590	45.870	46.220	45.260	...
1116+215.....	<45.470	45.890	46.250	44.740	...
1121+422.....	<45.730	45.480	45.580	...	...
1137+661.....	<46.460	46.120	46.730	45.730	45.880
1202+281.....	45.560	45.420	45.380	44.980	...
1211+143.....	45.410	45.410	45.640	45.620	44.710
1217+023.....	45.670	45.450	46.000	44.960	45.300
1226+023.....	46.440	46.480	46.790	45.480	46.020
1307+085.....	45.320	45.290	45.780	44.640	44.920
1351+640.....	45.590	45.250	45.430	...	...
1407+265.....	46.780	46.840	47.040	46.450	46.190
1416−129.....	<45.420	44.750	45.410	44.900	44.880
1426+015.....	45.190	45.180	45.640	44.830	44.700
1501+106.....	44.680	44.540	44.720	44.030	44.150
1613+658.....	45.690	45.420	45.530	44.830	...
1704+608.....	46.270	46.240	46.310	44.410	...
1721+343.....	45.700	45.560	46.070	45.060	45.470
1803+676.....	<44.940	45.280	45.520	43.650	...
2130+099.....	45.100	45.090	45.160	43.750	44.040
2135−147.....	45.660	45.570	45.780	44.940	45.340
2304+042.....	44.100	44.160	...	...	...

[a] The luminosities in the table are log νL_ν, in ergs s^{-1}.

with decreasing X-ray luminosity and the correlation between L_x and L_{opt} (regression slope $= 0.74 \pm 0.15$, which is in agreement with the Wilkes et al. 1994 slope of 0.71). We do not find the correlation between α_{ouv} and α_x reported by Puchnarewicz et al. (1996) or that of α_{ox} with α_x also reported by Laor et al. (1997; see § 4.1.5).

The mean SEDs for high- and low-luminosity quasars in our sample are shown separately in Figure 12. The quasars that contribute to the high-luminosity mean are 0637−752, 1226+023, 1407+265, and 1704+608 [L(0.8–1.6 μm) > 45.5], and those that contributed to the low-luminosity mean are: 0007+106, 0026+129, 0804+761, 1416−129, 1501+106 [L(0.8–1.6 μm) < 44.2], and EW(Hβ) > 70 Å. The low-luminosity object 1001+054 was omitted while making the mean, as we had no information on the X-ray slope, and the large errors in starlight caused large uncertainties in the $\sim$1 μm region. The higher luminosity SEDs show less dispersion around the median in the IR–UV bands than the lower luminosity SEDs. The range in X-rays is systematically shifted to lower X-rays for the higher luminosity SEDs, and the BBB is stronger (in the UV) for lower luminosity SEDs (meaning, as was also noticed from the slope analysis, that the peak of the BBB moves from the EUV into the UV as the luminosity increases). However, the range in the SEDs present is broad and overlaps significantly between the two samples.

4. DISCUSSION

4.1. *The Baldwin Effect*

In a simple, radiation-bounded photoionization model, one would expect the line flux in the HILs such as C IV and Lyα to be proportional to the strength of the ionizing continuum as a larger fraction of emitting material reaches the ionization state of the line. Since the EW is the ratio of line flux to that in the local continuum (i.e., in the same wave-

TABLE 11

OCTAVE LUMINOSITIES[a]

NAME	LUMINOSITY					
	0.8–1.6 μm	0.4–0.8 μm	0.2–0.4 μm	0.1–0.2 μm	0.15–0.3 keV	1–2 keV
0007+106.....	44.470	44.640	44.970	45.020	43.650	44.140
0026+129.....	44.870	45.010	45.230	45.340	44.250	44.350
0044+030.....	45.580	45.470	45.640	45.640	...	...
0050+124.....	44.770	44.750	44.830	44.650	44.630	43.890
0054+145.....	44.880	45.010	45.150	45.070	43.570	44.120
0133+207.....	45.090	45.030	45.420	45.650	45.030	45.030
0134+329.....	45.020	45.260	45.580	45.660	44.510	44.760
0205+024.....	44.570	44.870	45.260	45.320	44.110	44.010
0312−770.....	44.760	45.120	45.260	45.680	43.610	44.350
0637−752.....	46.230	46.330	46.460	46.720	<44.960	45.540
0804+761.....	44.700	44.880	45.310	45.310	44.190	44.180
0837−120.....	44.630	44.690	45.070	45.400	44.470	44.760
0844+349.....	44.100	44.470	44.770	44.760	42.850	43.230
0903+169.....	<45.480	44.980	44.910	45.180	44.050	44.470
0915+165.....	43.610	43.590	43.750	43.570	42.450	42.990
0923+392.....	<46.030	<46.100	45.950	46.110	44.680	45.180
1001+054.....	44.790	44.330	45.000	44.870	...	0.000
1004+130.....	45.190	45.470	45.860	45.730	...	0.000
1012+008.....	44.780	44.800	44.970	45.260	...	0.000
1028+313.....	44.590	44.730	44.960	45.250	43.930	44.300
1100+772.....	45.270	45.460	45.730	45.870	44.740	44.740
1116+215.....	45.200	45.390	45.790	45.950	44.220	44.220
1121+422.....	44.810	45.010	45.160	...	...	...
1137+661.....	45.630	45.940	46.210	46.430	45.150	45.400
1202+281.....	44.410	44.500	44.940	45.050	44.470	44.390
1211+143.....	44.760	44.960	45.220	45.200	45.190	44.370
1217+023.....	44.890	45.280	45.680	45.480	44.330	44.740
1226+023.....	45.870	46.030	46.320	46.440	44.850	45.330
1307+085.....	44.740	45.010	45.300	45.450	44.100	44.190
1351+640.....	44.490	44.790	45.040	44.960	...	...
1407+265.....	46.040	46.240	46.570	46.720	45.960	45.800
1416−129.....	44.210	44.450	45.020	45.060	44.360	44.450
1426+015.....	44.530	44.660	45.120	45.390	44.300	44.200
1501+106.....	43.680	43.820	44.290	44.410	43.540	43.610
1613+658.....	44.560	44.750	45.090	45.180	44.310	44.220
1704+608.....	45.510	45.640	45.810	45.940	43.750	44.250
1721+343.....	44.940	45.210	45.600	45.750	44.430	44.850
1803+676.....	44.640	44.760	45.060	45.150	42.810	43.800
2130+099.....	44.120	44.340	44.740	44.810	43.240	43.420
2135−147.....	44.860	45.200	45.380	45.220	44.340	44.560
2304+042.....	43.640	43.990	...	...	...	...

[a] The luminosities in the table are log νL_ν, ergs s^{-1}.

length region as the line), the Baldwin effect indicates that the line flux is increasing more slowly than the local continuum (or is constant). One possible interpretation is that the ionizing/heating continuum for the emission line (i.e., its driving continuum) is increasing more slowly than the local continuum, suggesting that the continuum shape correlates with the luminosity of a quasar. A number of papers have reported such a correlation. Tananbaum et al. (1986), Wilkes et al. (1994), and Green et al. (1995) note that the power law between UV and soft X-rays, α_{ox}, increases significantly with luminosity. This results in the soft X-ray luminosity being weaker relative to the UV in higher luminosity quasars.

4.1.1. *Zheng & Malkan Model*

Zheng & Malkan (1993), studying optical and UV properties of quasars and Seyfert galaxies, interpreted their color-luminosity relations as the result of a shift of the BBB toward lower energies in higher OUV luminosity objects. In this scenario higher luminosity quasars are predicted to have a lower fraction of higher energy ionizing photons available relative to the optical/UV continuum. This change in continuum shape would cause the EWs of high-ionization emission lines sensitive to the X-ray continuum, such as C IV and He II, to decrease at high luminosities relative to lower ionization emission lines, such as Lyα, C III], and the Balmer lines. The scenario predicts a stronger and more easily detectable Baldwin effect for higher ionization lines. We do see a shift in the SEDs, but our data do not favor this model, as we see the Baldwin effect in both HILs and LILs.

4.1.2. *Mushotzky & Ferland Model*

Mushotzky & Ferland (1984) explain the Baldwin effect as due to a systematic decrease in ionization parameter, U, as the luminosity increases. As the ionization parameter

TABLE 12

BROADBAND LUMINOSITIES

Name	L_{UVOIR} [a]	L_{bol} [b]	Lyman Continuum[c]	L_{Ion} [d]
0007+106.....	45.750	45.920	45.320	44.730
0026+129.....	45.920	46.120	45.640	45.200
0044+030.....	46.340	46.370	...	...
0050+124.....	46.000	46.100	45.320	44.690
0054+145.....	46.100	46.220	45.490	45.000
0133+207.....	46.540	46.750	46.170	45.630
0134+329.....	46.790	46.920	45.930	45.490
0205+024.....	45.970	46.170	45.720	45.290
0312−770.....	46.010	46.240	45.780	45.510
0637−752.....	47.370	47.550	46.920	46.560
0804+761.....	46.020	46.160	45.550	45.150
0837−120.....	45.920	46.220	45.870	45.390
0844+349.....	45.430	45.490	44.610	44.320
0903+169.....	46.020	45.790	45.550	45.060
0915+165.....	45.000	45.050	43.890	43.370
0923+392.....	46.810	47.100	46.390	45.940
1001+054.....	45.720	45.780	44.880	44.570
1004+130.....	46.460	46.550	45.690	45.430
1012+008.....	45.760	45.770	...	...
1028+313.....	45.730	46.040	45.720	45.270
1100+772.....	46.440	46.630	46.150	45.780
1116+215.....	46.440	46.580	45.980	45.720
1121+422.....	46.020	...	...	...
1137+661.....	46.850	47.110	46.720	46.320
1202+281.....	45.940	46.110	45.550	45.020
1211+143.....	45.980	46.260	45.920	45.330
1217+023.....	46.240	46.430	45.850	45.360
1226+023.....	47.080	47.280	46.690	46.280
1307+085.....	46.000	46.160	45.660	45.270
1351+640.....	45.920	46.000	44.920	44.650
1407+265.....	47.380	47.640	47.270	46.830
1416−129.....	45.500	45.810	45.500	44.910
1426+015.....	45.870	46.090	45.640	<45.530
1501+106.....	45.130	45.350	44.930	44.420
1613+658.....	46.040	46.170	45.480	<45.190
1704+608.....	46.750	46.820	45.910	45.670
1721+343.....	46.310	46.510	46.010	45.530
1803+676.....	45.870	45.740	45.050	44.760
2130+099.....	45.600	45.730	45.110	44.720
2135−147.....	46.160	46.320	45.720	<45.280
2304+042.....	44.620	...	...	...

[a] UV/OIR luminosity between 100 and 0.1 μm.
[b] Bolometric luminosity 1 m–10 keV.
[c] Lyman continuum 912 Å–10 keV.
[d] Ionizing photon rate multiplied by 1 Ryd. As 1 Ryd $= R = 2.18 \times 10^{-11}$ ergs, $N_{Ion} R = 10^{44} N_{44}$ ergs s^{-1} and $N_{Ion} = 4.6 \times 10^{54} N_{44}$ photons s^{-1}.

depends on the number of ionizing photons, U depends on the continuum shape. Their model assumes a single-zone BLR, i.e., determines the ionization for one "slab" at a given distance from the central source and assumes spherical symmetry. The model predicts the presence of a Baldwin effect for the C IV line, as the C IV luminosity increases rapidly with increasing U (decreasing UV luminosity and α_{ox}) in the range 30–32 in L_{1450} (log L_ν[2450 Å]). This relation flattens around $L_{1450} < 30$ and so predicts a weaker/or no Baldwin effect for lower luminosity active galactic nuclei (AGNs; see Fig. 1 in Mushotzky & Ferland 1984). In addition, their calculation showed that there should *not* exist a Baldwin effect in Lyα, C III], Hα, and Hβ lines, as the luminosity of these lines decreases with increasing U (i.e., decreasing luminosity) in the same luminosity range. It also follows that the EWs of Lyα, C III], and C IV should, in this scenario, be relatively independent of both α_{ox} and α_x, as the lines do not originate in the X-ray heated zones deep in the emission-line clouds.

In our sample this model matches only the C IV line, for which we see the Baldwin effect for $L_{1450} > 29.7$ [L(0.1–0.2 μm) > 45]. The four narrow-line low-luminosity AGNs that have L(0.1–0.2 μm) < 45 destroy the anticorrelation (with these objects the probability of a chance correlation is $P > 5\%$, without $P < 1\%$) and fall into the region where the model predicts no Baldwin effect (as it is the region where C IV remains fairly constant with increasing U). However, we see a strong correlation for EW(C IV) with α_{ox}, as well as less significant correlations for Lyα, Hβ, and O VI with spectral shape, none of which are consistent with the Mushotzky & Ferland model. Our data also show a Baldwin effect for Lyα and the Balmer lines that the model does not predict. The model also predicts that the C IV/Lyα ratio should decrease with increasing luminosity, but no such relation is found in our sample. We conclude that this model does not provide a good explanation for the relations present in our sample and so reject a pure photoionization scenario for the BELR.

4.1.3. *The Accretion Disk Model*

Netzer (1985, 1987) and Netzer, Laor, & Gondhalekar (1992), using an optically thick and geometrically thin accretion disk, explain the Baldwin effect in a different way. The model assumes a distribution of identical clouds at distances from the center of the disk greater than the size of the UV-emitting part of the disk. The incident ionizing flux from the accretion disk (AD) is composed of two components: the UV continuum, which is viewing-angle dependent because of limb darkening and change in projected surface area, and the X-ray component, which is viewing-angle independent. The UV emission is strongest when the disk is viewed face-on. Because the BELR radiates more isotropically than the UV disk, a random selection of objects differing only in viewing angle would result in measurements of constant line luminosities but varying UV continuum luminosities, producing an anticorrelation of EW with L_{UV}. In addition, an anticorrelation between EW and α_{ox} is expected, as objects viewed face-on would have steeper α_{ox} (due to relatively higher UV–to–X-ray emission) and smaller EW than those seen edge-on. Correlations of the more isotropic X-ray emission with line EW would be much weaker.

The continuum viewed by the BELR clouds themselves is a function of viewing angle. As a result, clouds at small viewing angles produce strong Lyα, O VI, and Balmer continuum emission because of the stronger UV ionizing continuum. Clouds at large viewing angles, where the fraction of high-energy X-ray photons is largest, emit low-excitation lines such as Fe II and Mg II. The model predicts that in clouds at these viewing angles, Fe II emission can reach an intensity comparable with that of Lyα and more than 10 times that of Hβ. Under our assumption of optically thin emitting clouds, this viewing-angle dependence will not affect the observed line strengths unless external effects, such as viewing-angle–dependent reddening, are also present.

In general the results presented here show good agreement with the predictions of the AD model. We see an anticorrelation of EW with UV luminosity for Lyα, Hβ, Hδ, and a less significant relation for C III], although this

TABLE 13

PROBABILITY OF A CHANCE CORRELATION BETWEEN LINE EW AND CONTINUUM LUMINOSITY PARAMETERS[a]

Variable	Lyα N v	Lyβ O vi	C iv	Si iv O iv]	Al iii C iii]	Hβ	[O iii]	Fe ii	Hγ	Hδ	[Ne iii]	[NeHe]	[O ii]	[Ne v]	Mg ii
L_{UVOIR}[b]	2.0, 3.1	...	...	...	...	**0.5, 0.8**	5.1, 5.4	...	**0.6, 0.6**	2.1, 1.5	...	...	...	...	...
L_{bol}[c]	1.5, 2.4	...	...	...	4.9, 1.5	**0.8, 1.5**	...	...	**0.8, 1.0**	...	...	...	...	...	...
L_{Ly} continuum[d]	4.0, 5.3	...	...	...	**1.4, 1.8**	2.3, 4.7	...	...	...	...	...	...	...	...	...
L_{Ion} continuum[e]	1.2, 1.6	...	...	...	**1.8, 0.3**	**0.8, 1.5**	...	...	...	...	...	...	...	...	...
L(10–100 μ)	...	...	...	...	...	**0.2, 0.4**	...	...	**1.7, 1.1**	**0.7, 0.5**	...	...	...	...	...
L(1–10 μ)	5.1, 4.9	4.8, 3.0	...	...	...	4.0, 5.2	...	...	**1.2, 1.4**	*1.0, 0.8*	...	...	...	...	...
L(0.1–1 μ)	**0.4, 0.6**	...	...	...	5.0, 1.6	**0.9, 1.1**	...	3.0, 3.5	...	...	...	...	...	...	...
L(0.1–1 keV)	...	...	...	...	...	...	...	...	...	...	...	...	...	...	...
L(1–10 keV)	...	...	...	...	4.0, 0.3	**0.3, 0.6**	...	2.9, 2.7	...	2.4, 2.0	...	...	...	...	...
L(0.8–1.6 μ)	3.4, 3.6	...	...	...	...	4.9, 5.7	3.1, 5.6	...	**1.7, 1.1**	3.7, 3.0	...	2.0, 2.4	...	...	...
L(0.4–0.8 μ)	**1.2, 1.7**	...	...	...	...	***0.2, 0.3***	...	...	***1.1, 1.4***	...	...	...	...	...	...
L(0.2–0.4 μ)	1.1, 1.5	...	...	...	...	2.4, 2.0	...	3.5, 4.3	...	...	...	...	...	...	...
L(0.1–0.2 μ)	***0.4, 0.6***	...	...	...	2.4, 0.7	**1.3, 1.6**	...	3.0, 5.0	...	...	...	...	...	...	...
L(0.15–0.3 keV)	...	...	...	...	...	...	...	...	...	...	...	...	...	...	...
L(1–2 keV)	...	...	...	...	***0.9, 0.2***	...	...	2.1, 3.5	...	...	...	...	...	...	...
L_{opt}	**1.3, 2.0**	1.7, 3.8	...	...	3.3, 1.1	**0.4, 0.5**	...	...	...	**1.5, 1.6**	...	...	...	...	3.0, 2.9
L_x	...	...	...	...	**1.0, 0.3**	...	...	...	...	...	...	...	...	...	...
$C_{UV/IR}$	...	...	...	...	...	...	...	...	...	1.7, 2.4	...	...	...	...	...
α_{ox}	5.2, 4.5	3.1, 4.1	**1.2, 0.9**	...	...	2.3, 1.4[f]	...	...	...	...	...	...	5.0, 4.1	...	...
α_x	...	...	...	...	...	...	...	...	...	...	...	...	...	...	...
α_{ouv}	...	...	...	...	...	...	...	...	...	...	...	**1.3, 1.8**	...	...	...

[a] P_1, P_2 are the percentage probabilities of a chance correlation obtained by the generalized Kendall & Spearman rank tests; italicized values indicate primary correlations; ellipses indicate probabilities greater than 5.0%.

[b] UV/OIR luminosity between 100 and 0.1 μm.

[c] Bolometric luminosity 1 m–10 keV.

[d] Ly continuum 912 Å–10 keV.

[e] Ionizing photon rate multiplied by 1 Ryd. As 1 Ryd $= R = 2.18 \times 10^{-11}$ ergs, $N_{Ion} R = 10^{44} N_{44}$ ergs s^{-1} and $N_{Ion} = 4.6 \times 10^{54} N_{44}$ photons s^{-1}.

[f] Correlation becomes more significant ($P_1 = 0.55\%$, $P_2 = 0.31\%$) if quasar 1001+054 is omitted. However, there is no obvious reason to omit this object.

TABLE 14

THE PROBABILITY OF A CHANCE CORRELATION BETWEEN LINE FLUX AND CONTINUUM FLUX PARAMETERS[a]

Variable	Lyα N v	Lyβ O vi	C iv	Si iv O iv]	Al iii C iii]	Hβ	[O iii]	Fe ii	Hγ	Hδ	[O ii]	Mg ii
F(10–100 μm)	…	…	…	…	…	2.3, 2.9	**0.9, 1.1**	**0.2, 0.5**	…	…	…	…
F(1–10 μm)	**1.5, 0.9**	…	…	…	**0.7, 1.5**	**0.09, 0.15**	**0.1, 0.3**	**0.01, 0.08**	**0.2, 0.8**	1.8, 2.3	…	…
F(0.1–1 μm)	**0, 0**[b]	…	**1.7, 1.7**	**0.3, 0.5**	**0.6, 0.8**	**0.0, 0.01**	**0, 0.01**	**0, 0**	**0, 0**	**0, 0**	…	…
F(0.1–1 keV)	**1.6, 1.4**	…	**0.8, 1.4**	…	**1.9, 0.9**	**0.3, 0.5**	**1.3, 1.7**	5.0, 5.1	**1.5, 1.6**	2.0, 2.9	…	…
F(1–10 keV)	…	…	**0.9, 1.4**	…	…	…	**0.8, 1.4**	4.7, 5.1	…	3.6, 2.9	2.5, 1.7	
F(0.8–1.6 μm)	**0.04, 0.04**	…	…	***0.5, 0.6***	***0.3, 0.5***	**0.02, 0.04**	**0.1, 0.2**	**0.06, 0.11**	**0.02, 0.05**	**0.05, 0.15**	…	…
F(0.4–0.8 μm)	**0.08, 0.11**	…	…	**1.0, 1.3**	2.6, 2.5	**0.02, 0.03**	**0.02, 0.03**	**0.01, 0.04**	**0, 0**	**0, 0.01**	…	…
F(0.2–0.4 μm)	**0.01, 0.03**	…	2.8, 3.1	**0.3, 0.9**	**0.6, 1.2**	***0, 0.01***	***0, 0***	**0, 0.01**	***0, 0***	**0, 0**	…	…
F(0.1–0.2 μm)	***0, 0***	…	**0.3, 0.3**	**0.8, 0.9**	**1.3, 0.7**	**0.02, 0.02**	**0.02, 0.05**	***0.01, 0.01***	**0, 0**	***0, 0***	…	…
F(0.15–0.3 keV)	…	…	…	…	**1.3, 1.0**	**0.4, 0.5**	**0.7, 1.0**	2.3, 3.0	**0.9, 0.9**	**1.50, 1.97**	…	…
F(1–2 keV)	**0.8, 1.0**	…	***0.9, 0.6***	2.3, 3.5	4.7, 2.9	**0.2, 0.2**	**0.4, 0.3**	…	**0.4, 0.6**	**0.4, 0.8**	…	…
$F_{\rm DRIV}$[c]	**0, 0**	3.2, 2.9	**0.27, 0.33**	…	**0.41, 0.35**	**0.08, 0.08**	…	2.9, 3.5	**0.01, 0.04**	**0.01, 0.03**	…	…
Driving/heating	Ly con[e],	He i con[f]	Ly con	…	Ly con	Ly, He i con	…	>800 eV	Ly, He i con	Ly, He i con	…	600–800 eV
Continuum[d]	300–400 eV		300–400 eV			300–800 eV			300–800 eV	300–800 eV		

[a] Primary correlations are italicized.

[b] 0 denotes probability less than 10^{-4}.

[c] $F_{\rm DRIV}$ driving continuum flux; see footnote d.

[d] Driving/heating continua after Krolik & Kallman (1998) Table 4; for Si iv, [O iii], and [O ii] driving continua are not known.

[e] "Ly con" denotes Lyman continuum: 13.6–24.5 eV.

[f] "He i con" denotes He i continuum: 24.5–54.4 eV.

TABLE 15

CORRELATIONS

Variables	Number of Correlations Tested	Number of Random, Significant Correlations Expected	Number of Significant Correlations Found
EW vs. continuum parameters	315	6	31
FWHM vs. continuum parameters.....	315	6	2
EW vs. line EW	105	2	8
FWHM vs. line FWHM	105	2	8
EW vs. FWHM of same line	15	0.3	1
Line flux vs. continuum flux	131	3	68
Line flux vs. driving continuum	8	0.2	6
Sum	995	20	124

becomes significant after excluding the low-luminosity narrow-line AGNs (probably NLSy1; see § 3.1.1). A similar relation for C IV (the traditional Baldwin effect) also appears when these NLSy1s are omitted. We see a strong correlation between EW and α_{ox} for C IV *only* and less significant relations for Lyα, Hβ, and probably for O VI (although we do not have enough data to draw strong conclusions here). None of the lines correlate with X-ray luminosity, agreeing with the model predictions.

To make a more quantitative comparison between the model and our data, we assume that the AD and BELR are hidden by a dusty torus similar to that postulated for Sy1 and Sy2 galaxies. Adopting an opening angle of $\sim 60^\circ$ (Phillips, Charles, & Baldwin 1983) and following Netzer et al. (1992), the AD model predicts that the range in disk inclination yields a range in OUV luminosity of a factor of 2 (0.3 in log). This modifies the slope α of the line luminosity versus driving continuum correlations in the following way:

$$\alpha = 1 - 0.3/(\log F_{\rm cont}^{\rm max} - \log F_{\rm cont}^{\rm min}) .$$

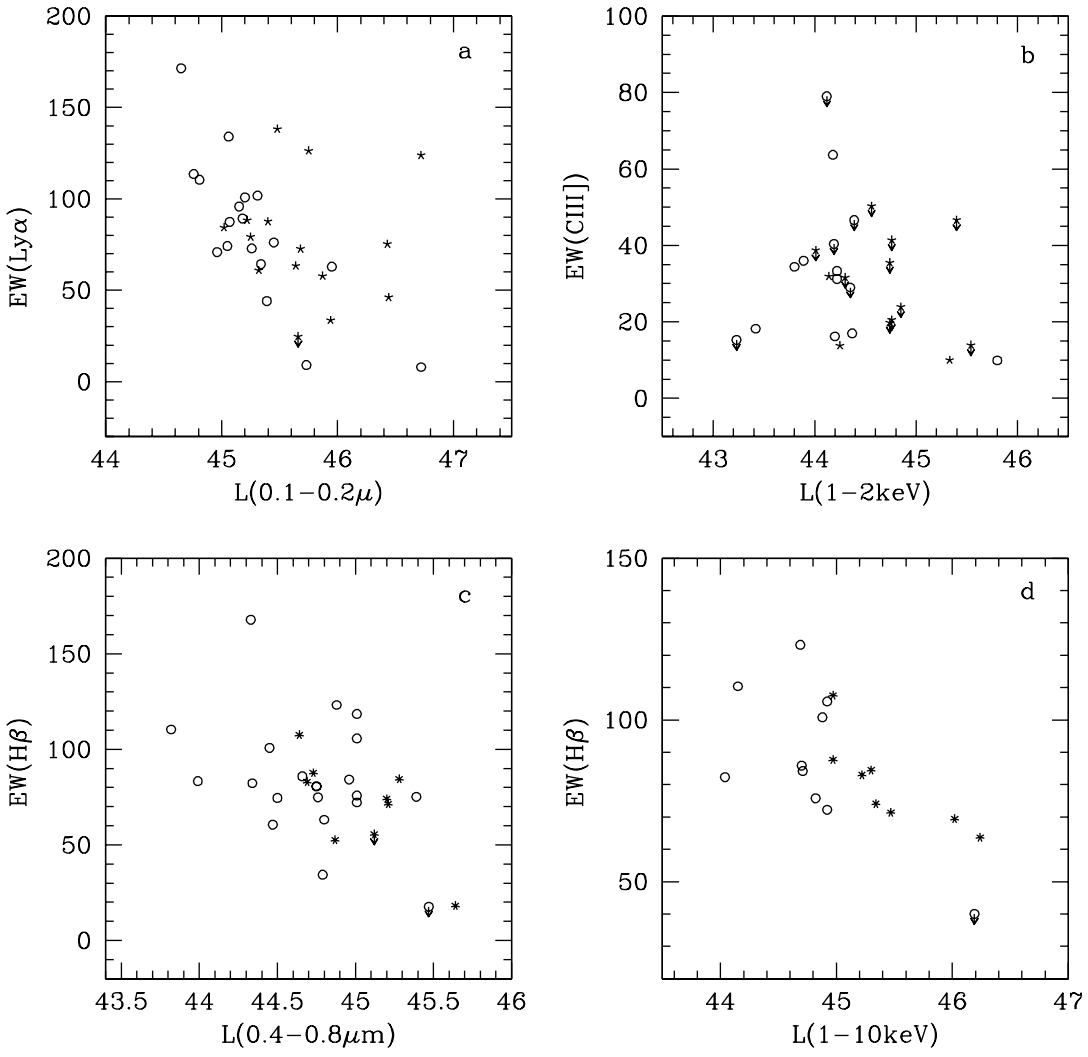

FIG. 4.—Primary correlations for UV and optical line EWs vs. continuum luminosities. RLQs are indicated by stars and RQQs by circles.

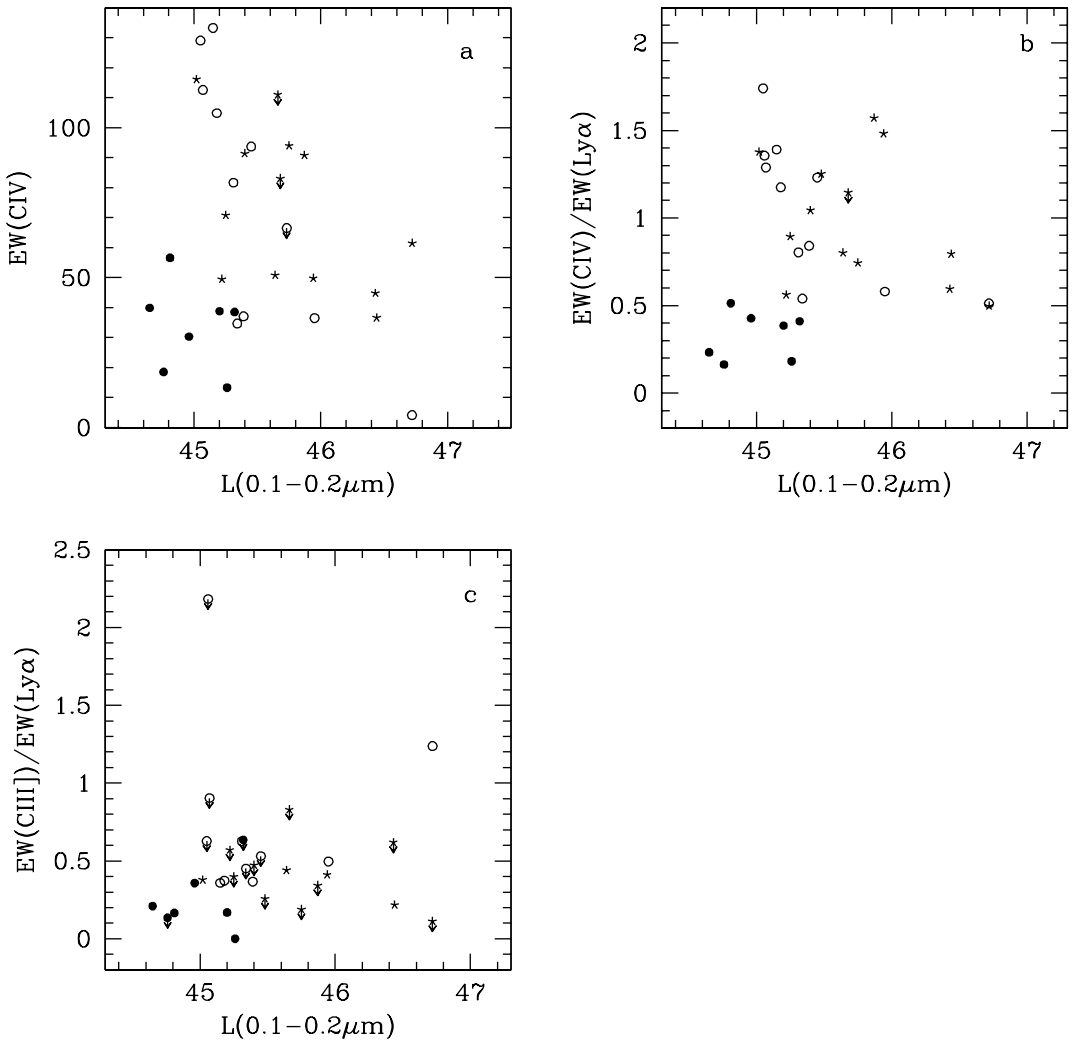

FIG. 5.—(*a*) Lack of Baldwin effect for EW(C IV). (*b*) C IV/Lyα and (*c*) C III]/Lyα vs. UV luminosity relations. Filled circles denote NLSy1s, which decrease the significance of the C IV Baldwin effect in our sample.

The range in flux continuum $F_{\rm cont}$ in our sample is $\sim$2.5 orders of magnitude, so the expected slope is $\sim$1–0.12 = 0.88. Most of the lines fit into this scenario (Lyα, Hγ, and probably Hβ, Hδ, Fe II, O VI, although the errors are large; see Table 16). However, C IV and C III] have flatter slopes (0.57 ± 0.14 for C IV and 0.69 ± 0.19 for C III]). Exclusion of the seven discrepant NLSy1 objects (see § 3.1.1) yields slopes still not steep enough (0.64 ± 0.14 for C IV and 0.64 ± 0.25

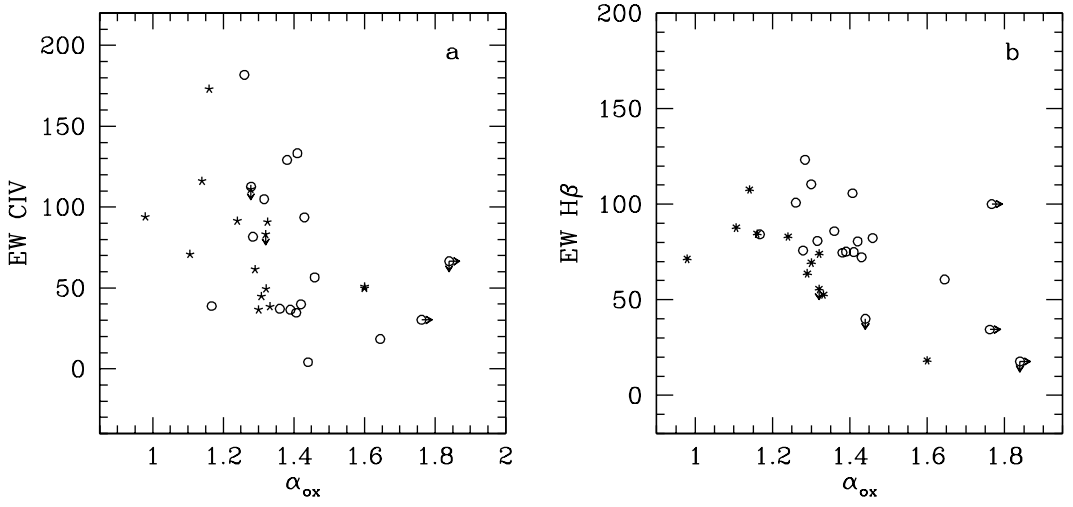

FIG. 6.—(*a*) EW(C IV) vs. α_{ox} correlation. (*b*) EW(Hβ) vs. α_{ox} relation. Notice quasar 1001+054 in the upper right corner, which drastically spoils this correlation.

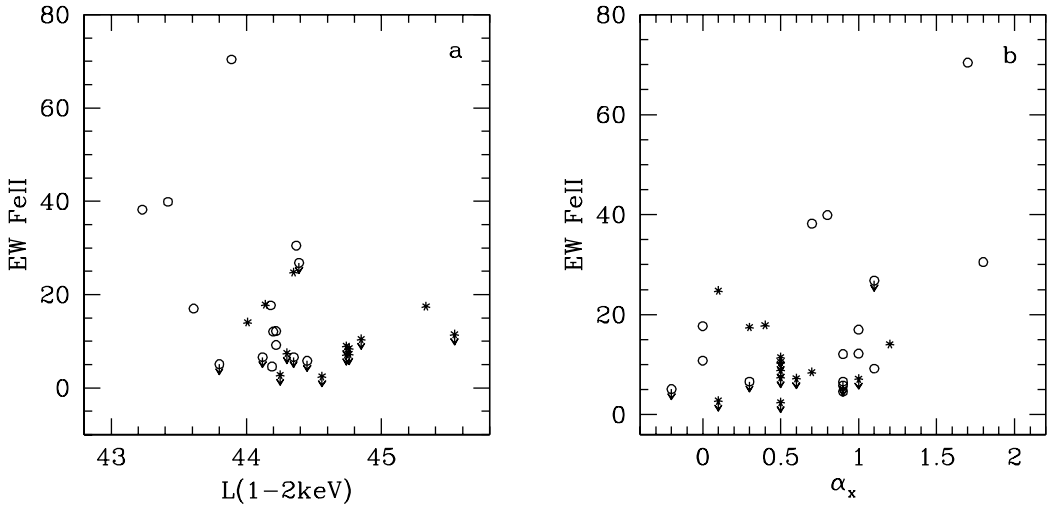

FIG. 7.—(*a*) Relation between the EW(Fe II) and the soft X-ray luminosity. (*b*) The relation between EW(Fe II) and α_x. We see no correlations but rather zones of avoidance such that objects with stronger X-ray luminosities and/or flat spectra do not have strong Fe II.

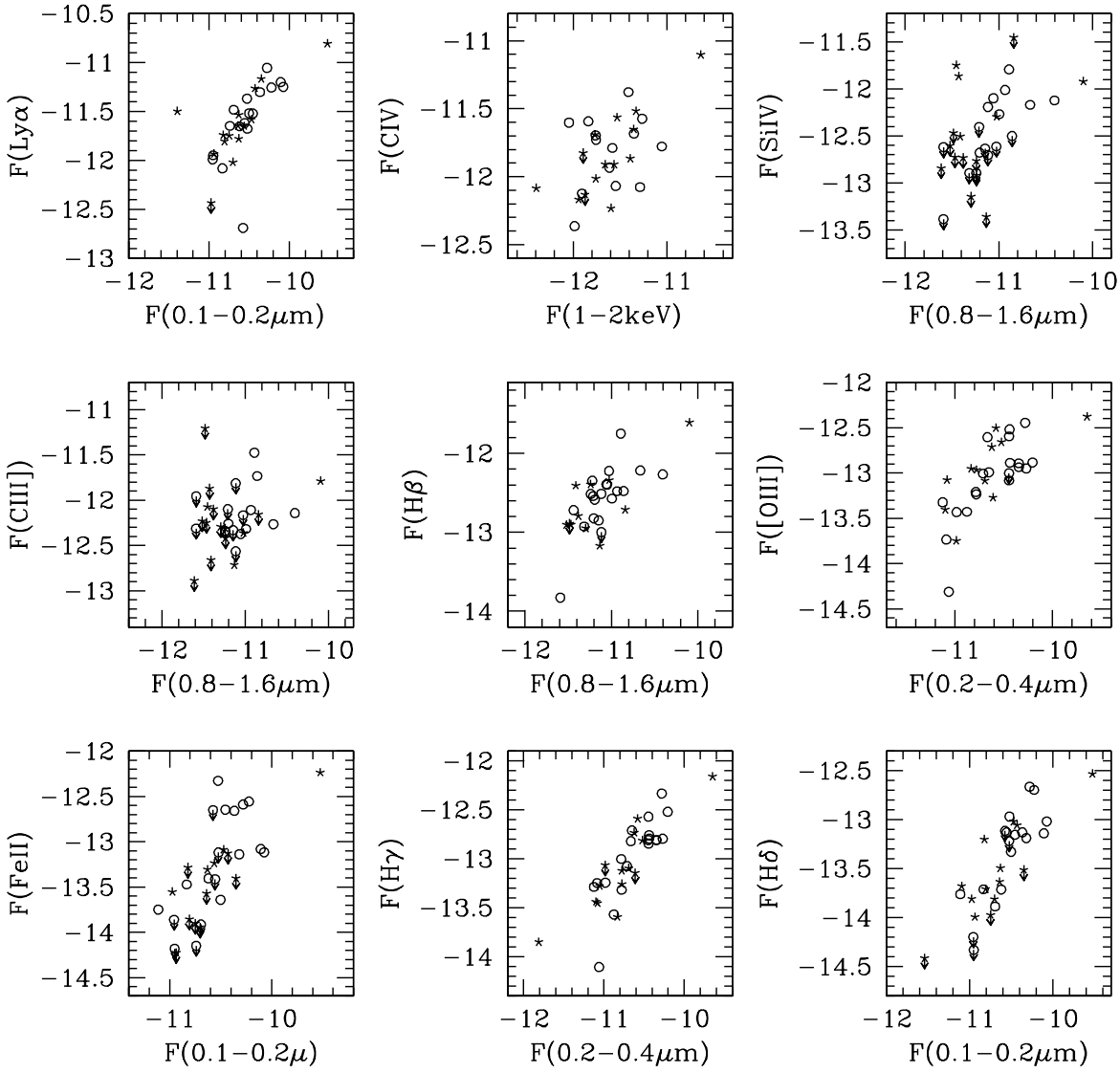

FIG. 8.—Primary correlations for the line vs. continuum fluxes

TABLE 16

REGRESSION SLOPES AND SCATTER IN LINE FLUX/CONTINUUM FLUX CORRELATIONS

Variable	Lyα N v	Lyβ O vi[a]	C iv	Si iv O iv[b]	Al iii C iii][b]	Hβ	[O iii]	Fe	Hγ	Hδ	[O ii]	Mg ii
F(0.8–1.6 μm)	0.64 ± 0.14	...	...	0.97 ± 0.21	0.51 ± 0.15	1.03 ± 0.24	0.79 ± 0.30	1.18 ± 0.19	0.76 ± 0.14	0.71 ± 0.27	...	...
F(0.4–0.8 μm)	0.60 ± 0.19	...	...	0.71 ± 0.28	0.36 ± 0.13	0.88 ± 0.13	0.85 ± 0.20	1.30 ± 0.16	0.81 ± 0.12	0.81 ± 0.15	...	...
F(0.2–0.4 μm)	0.61 ± 0.23	...	0.45 ± 0.22	0.74 ± 0.29	0.41 ± 0.19	1.05 ± 0.19	1.07 ± 0.15	1.30 ± 0.17	0.95 ± 0.11	1.08 ± 0.10	...	...
F(0.1–0.2 μm)	0.77 ± 0.33		0.55 ± 0.32	0.69 ± 0.48	0.39 ± 0.17	0.90 ± 0.22	0.81 ± 0.24	1.26 ± 0.17	0.86 ± 0.11	1.02 ± 0.10	...	...
F(0.15–0.3 keV)	...	...	...	...	0.18 ± 0.21	0.39 ± 0.18	0.21 ± 0.20	0.66 ± 0.23	0.43 ± 0.13	0.43 ± 0.24	...	...
F(1–2 keV)	0.57 ± 0.11	...	0.37 ± 0.16	0.79 ± 0.22	0.53 ± 0.21	0.77 ± 0.11	0.52 ± 0.22	...	0.69 ± 0.12	0.81 ± 0.21	...	...
$F_{\rm DRIV}$	0.88 ± 0.13	1.05 ± 1.12	0.57 ± 0.14	...	0.69 ± 0.16	1.07 ± 0.34	...	0.92 ± 0.36	0.83 ± 0.15	0.97 ± 0.21	...	...
σ primary correction[c]	0.37	...	0.52	0.50	0.62	0.30	0.28	0.28	0.24	0.28	...	...
σ driving continuum[d]	0.22	0.30	0.38	...	0.57	0.33	...	0.51	0.36	0.32	...	...

[a] Too few data to find primary correlation; line vs. $F_{\rm DRIV}$ slope, based on only nine objects.

[b] Si iv and C iii] line have more than 50% upper limits, so the scatter is overestimated and the slopes are unreliable.

[c] Scatter in the primary correlation defined as: $\sigma = \{1/(N-1) \sum_{i=1}^{n} [x_i - (y_i - b)/a]^2\}^{1/2}$, where $y = ax + b$, x_i is log of the continuum flux, and y_i is log of the line flux. The primary correlations are shown in Table 14.

[d] Scatter in the line/driving continuum relation, σ defined as in footnote c; the Fe ii multiplet has more than 50% of upper limits in the line/driving continuum relation, so scatter is overestimated and the slope is unreliable; regression slopes for C iv and C iii] lines are given, including NLS1 objects.

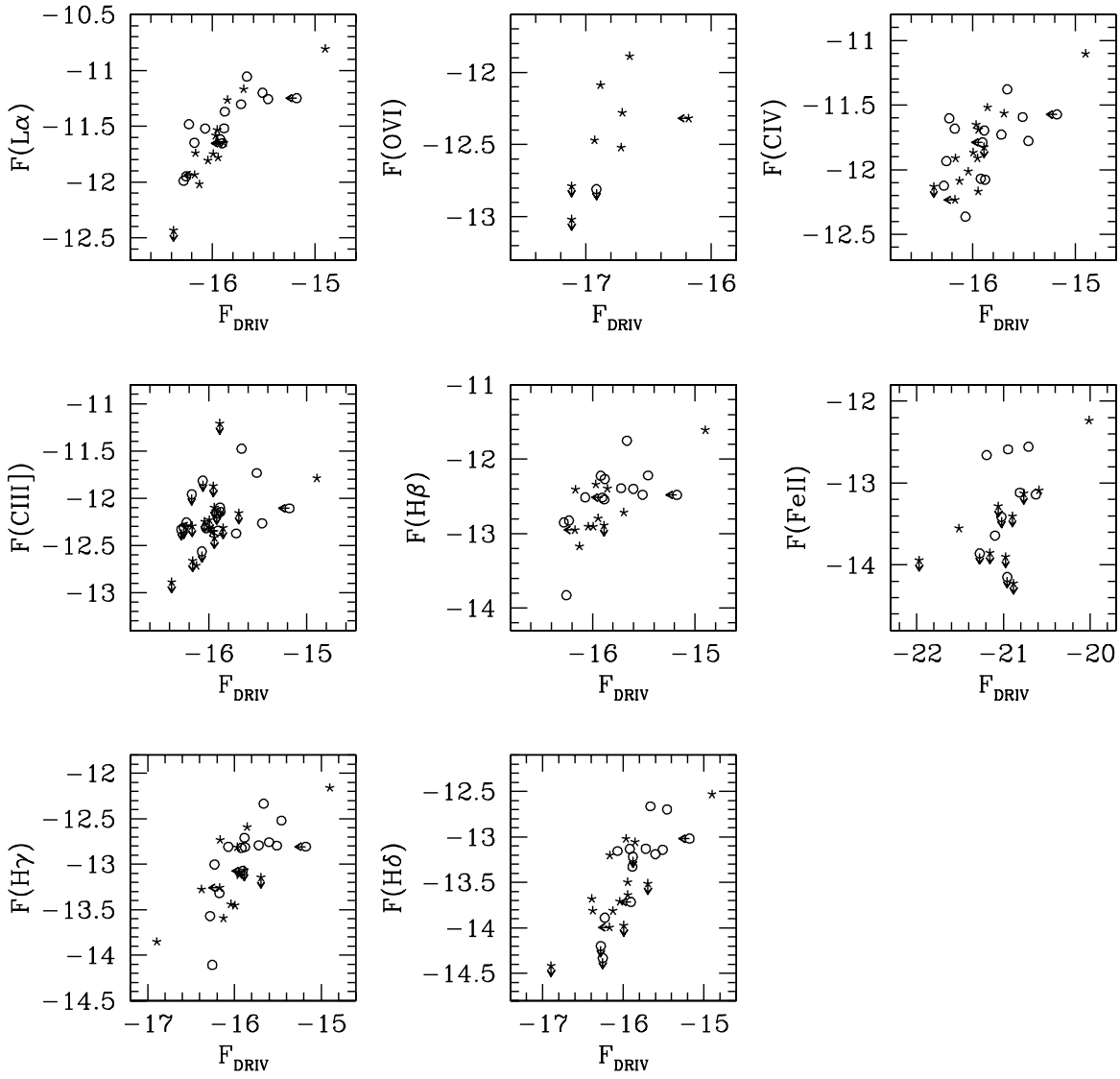

FIG. 9.—Correlations for UV and optical line fluxes vs. driving continuum fluxes

for C III]). (We note that the C III] line sample has greater than 50% upper limits, so the errors in the regression slopes are probably underestimated.) This may be due to a significant contribution from collisional excitation, which is not directly related to the ionizing continuum. In contrast, the Fe II line flux versus continuum flux correlations are too steep (~ 1.3; see Table 16) to fit this scenario. One possible explanation for this behavior is reddening by dust, which increases with increasing viewing angle. Given the predominance of Fe II emission from large viewing angles described above, this line would be reddened more than the continuum. This could lead to a stronger viewing-angle dependence than the continuum and so a steeper relation, as is observed.

TABLE 17

SUMMARY OF CORRELATIONS BETWEEN CONTINUUM PARAMETERS

log y	log x	α_1 ($y = x^{\alpha_1}$)	α_2 ($x = y^{\alpha_2}$)	$1/\alpha_2$
L(10–100 μm).....	L(1–10 μm)	1.01 ± 0.06	0.73 ± 0.06	1.37
L(10–100 μm).....	L(0.1–1 μm)	0.70 ± 0.10	0.71 ± 0.20	1.41
L(1–10 μm)	L(0.1–1 μm)	0.73 ± 0.08	0.97 ± 0.13	1.03
L(0.8–1.6 μm).....	L(0.4–0.8 μm)	0.95 ± 0.07	0.92 ± 0.06	1.07
L(0.4–0.8 μm).....	L(0.2–0.4 μm)	0.92 ± 0.05	0.94 ± 0.07	1.06
L(0.2–0.4 μm).....	L(0.1–0.2 μm)	0.88 ± 0.02	1.06 ± 0.04	0.94
L(0.1–0.2 μm).....	L(1–2 keV)	0.88 ± 0.08	0.84 ± 0.03	1.19
L(1–2 keV).....	L(1–10 keV)	1.04 ± 0.12	0.75 ± 0.06	1.33

Another discrepancy between our results and the predictions involves the scatter around the mean slope in the line versus continuum correlations, which is larger than that expected (i.e., greater than 0.15 around the mean; Table 16). Effects that could increase the scatter include a nonspherical geometry of the BLR clouds, random obscuration by dust in the NLR, or a different opening angle for the dusty torus. These possibilities are discussed in the following sections.

4.1.4. *The Two-Zone BELR*

The BLR is sometimes suggested to include two distinct regions: the HIL region (Lyα, C IV, C III]) and LIL region (Balmer, Fe II, and Mg II lines). Collin-Soufrin et al. (1988) assumed, for example, that the LILs have a disk geometry, while the HILs do not. In this scenario, a random selection

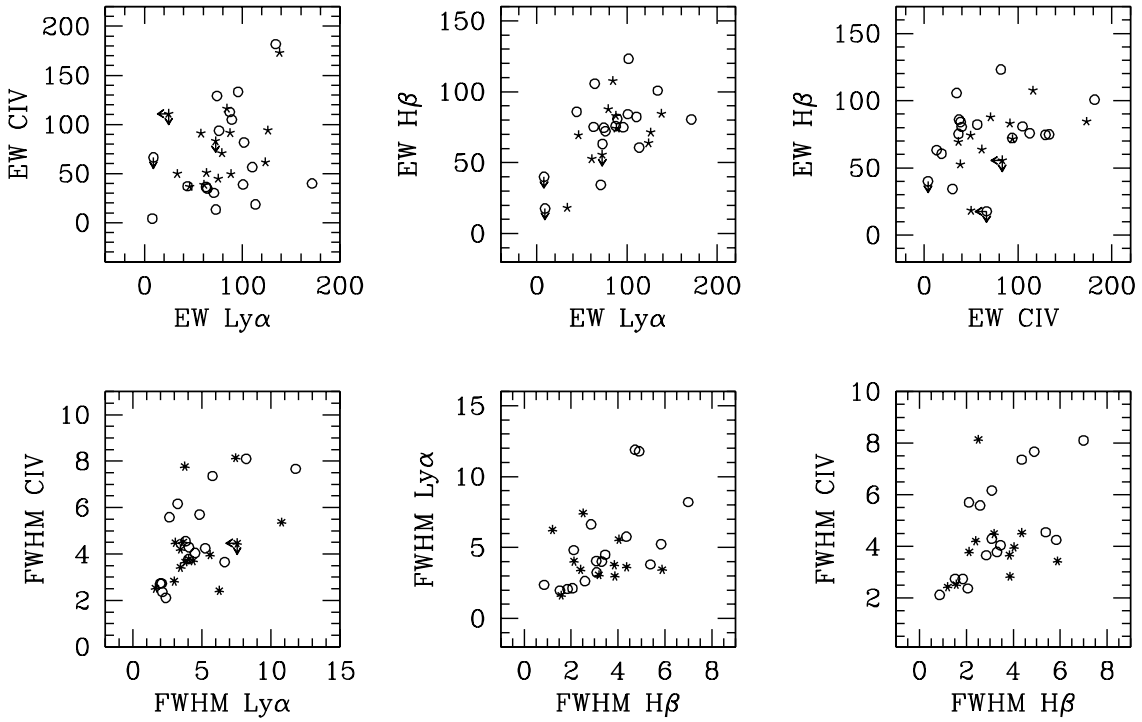

FIG. 10.—Correlations between the EW (in Å) and FWHM (in units of 10^{-3} km s^{-1}) of Lyα, C IV, and Hβ lines

of objects differing only in disk inclination would lead to a scatter around the mean in a plot of $F_{\rm line}$ versus $F_{\rm DRIV}$ that is larger and a slope that is flatter for the HILs (as these lines have a spherical symmetry) than for the LILs. In our sample the mean slopes for the LIL Balmer and Fe II lines are indeed steeper than those for the HILs (i.e. Lyα, C IV, and C III]; see Table 16). However, the scatter in the correlations is larger for LILs than HILs, which is contrary to the predictions. This scenario potentially offers an explanation for the steepness of the Fe II versus OUV flux correlations if distributions of Fe II and OUV continuum emission from the AD differ. However, given the partial agreement between model predictions and the observations and the large uncertainties in the derived slopes, we are unable to draw strong conclusions on the applicability of this model.

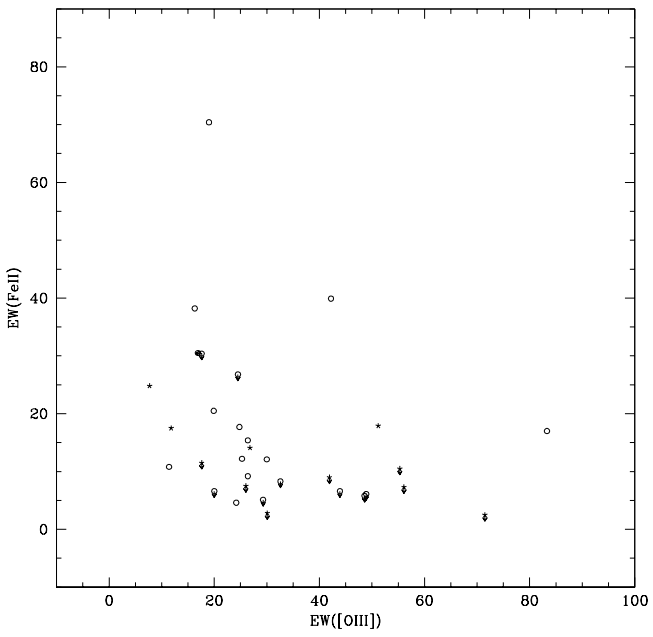

FIG. 11.—Correlation between [O III] and optical Fe II EWs (the first Boroson & Green eigenvector).

4.1.5. *The Role of Dust*

The presence of dust in quasars has been discussed by many authors (e.g., Webster et al. 1995; Rawlings et al. 1995; Sprayberry & Foltz 1992; Low et al. 1989; McLeod & Rieke 1994a, 1994b). Baker (1997), for example, studied a complete sample of RLQs and found correlations between optical continuum and emission lines and the orientation indicator R (the ratio of radio-core to lobe flux density). These correlations, and the result that core-dominated quasars are 3–5 mag brighter in the optical region than lobe-dominated quasars, were explained as due to viewing-angle–dependent dust extinction. In addition, strong correlations of the EWs of [O II] and Mg II and the [O II]/[O III] ratio with R, the lack of significant trends for C III], C IV, Hβ, and a weaker trend for [O III] suggest that the BLR and the inner part of the NLR suffer extinction similar to the continuum. The Balmer decrements (Hα/Hβ and Hβ/Hγ) also correlate with R, although for Hβ/Hγ the correlation is less significant, probably because of contamination of Hγ by [O III] λ4363. Given the lack of measured R values for the quasars in our sample, we can provide only weak, direct support for this scenario by confirming the lack of any relation between the Balmer decrement, Hβ/Hγ, and the EW of the broad emission lines expected from the above correlations with R.

Puchnarewicz et al. (1996), studying a sample of X-ray–selected Sy1 galaxies and quasars, covering a wide range in

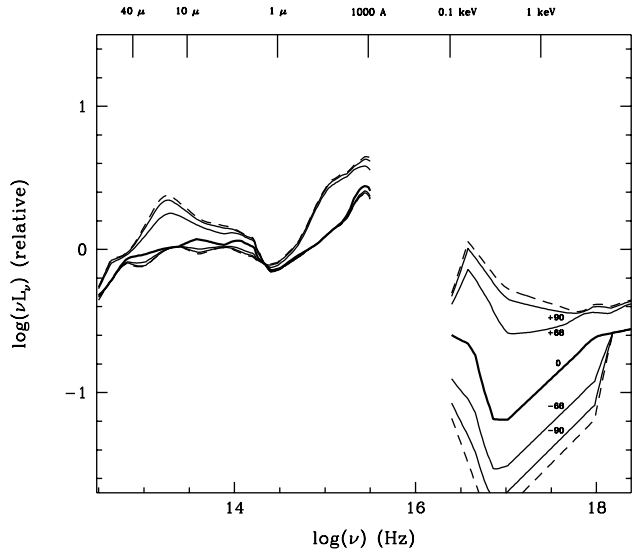

FIG. 12*a*

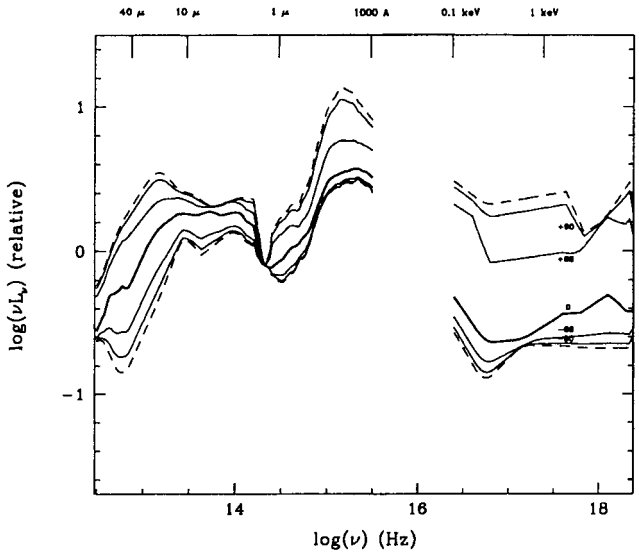

FIG. 12*b*

FIG. 12.—(*a*) Mean energy distributions for high-luminosity quasars, normalized at 1.5 μm and the 68, 90, and 100 (*dashed line*) Kaplan-Meier percentile envelopes. (*b*) Similar mean energy distributions for low-luminosity quasars.

redshift and X-ray spectral slope, reported that the optical–to–X-ray spectra change from convex to concave as the X-ray slope, α_x, hardens (i.e., α_x and α_{ox} anticorrelate). This was interpreted in terms of an intrinsic convex spectrum being absorbed by differing amounts of cold gas and dust, possibly depending on viewing angle and so similar to the Baker (1997) scenario. Given the small range of α_x in our sample (-0.3 to 0.9; see -2 to 3 for Puchnarewicz et al. 1996) and the large scatter in the correlation, we do not see a significant correlation here. However, dividing our sample according to α_x and applying the median test reveals a significant trend (greater than 99%) for α_{ox} to be smaller when α_x is hard. We do not find a significant correlation between α_{opt} (i.e., α_{ouv} in our sample) and α_x; again, this is not surprising given our small range of α_x. We also note that Puchnarewicz et al. (1996) show a weak correlation for the high-redshift objects only ($z > 1.0$, $P_S = 4\%$): their lower redshift objects do not show a correlation, which is consistent with our sample.

There are a number of other properties of our sample that could potentially be explained by dust reddening. These include the larger-than-canonical "case B" Balmer decrements $2.85 < \mathrm{H}\alpha/\mathrm{H}\beta < 7$ (case B $\mathrm{H}\alpha/\mathrm{H}\beta = 2.85$) and $2.1 < \mathrm{H}\beta/\mathrm{H}\gamma < 5.3$ (case B $\mathrm{H}\beta/\mathrm{H}\gamma = 2.1$), implying a reddening of $A_v < 2.04$ mag; the existence of primary correlations for optical and UV lines that are not with the driving continuum (see § 4.1.3); the increased scatter in the line luminosity versus driving continuum relations above that predicted by the disk model; and the larger scatter within the line/continuum correlation of Hγ compared with Hβ (see Table 16). We investigate dust as a contributor to the correlations in detail in the next section.

4.1.6. *Simulations of the Effects of Reddening*

We investigate the effects of dust on the results of our analysis by applying random amounts of dust reddening to a simulated sample of quasars with properties similar to our actual sample. First we selected the quasar in our sample with the largest BBB, i.e., the one with largest difference: L(0.1–0.2 μm) − L(0.8–1.6 μm) (PG 1426+015). Since this object also has a ratio Hβ/Hγ equal to the unreddened "case B" value (2.1), we assume it is unreddened. A hypothetical sample of 26 objects was then constructed with the continuum shape of PG 1426+015 but covering the range in bolometric luminosity present in the current sample [2.5 in L(0.8–1.6 μm)], spaced by 0.1 in log νL_ν. The maximum reddening was determined from the difference in strength of the strongest and weakest BBBs in the real sample. Assuming that the dust lies outside the BELR, a random amount of reddening up to the maximum was applied to both the SED and the two extreme emission lines (in λ), Lyα and Hβ. The process was performed twice, using two extinction curves: the standard Galactic extinction curve (Seaton 1979) and the Small Magellanic Cloud (SMC) extinction curve (Prévot et al. 1984), which corresponds well to the extinction by dust dominated by amorphous carbon grains (Czerny et al. 1995). The estimated maximum reddening was $E(B-V) = 0.32$ for the Seaton extinction curve and $E(B-V) = 0.20$ for the SMC extinction curve. We note that this is much less than that estimated from the Balmer decrement, implying a different amount of obscuration. We then performed a correlation analysis similar to that applied to the real sample to look for the primary correlations between Lyα and Hβ and various parts of the SED and to estimate the scatter in the resulting line versus driving continuum correlations. The results are as follows: for the Seaton extinction curve the primary correlation for Lyα was with the driving continuum and for Hβ with L(0.2–0.4 μm), the scatter for the line versus driving continuum correlation for Lyα was $\sigma = 0.12$ and for Hβ $\sigma = 0.42$; for the SMC extinction curve the primary correlation for Lyα was with L(0.1–0.2 μm) and for Hβ was with L(0.2–0.4 μm), the line versus driving continuum correlation scatter for Lyα was $\sigma = 0.12$ and for Hβ $\sigma = 0.20$.

A comparison of these results with the current sample (Tables 14 and 16) reveals that the simulation using the SMC extinction curve has the same primary correlations for Lyα and Hβ lines as the real sample, and the scatter in the line versus driving continuum correlations is comparable with the additional scatter required to bring the results into agreement with the AD model (see Table 16). The scatter

introduced by the Netzer AD model (§ 4.1.3) for both Lyα and Hβ is $\sigma = 0.15$. The addition of dust yields an overall scatter, $\sigma \sim 0.27$ for Lyα and $\sigma \sim 0.35$ for Hβ, which is slightly larger than in the real sample (compare with $\sigma = 0.22$ and $\sigma = 0.33$, respectively). However, this slightly larger scatter is probably due to the simplifying assumption that the difference between objects with larger BBB and those with smaller BBB is entirely due to dust, neglecting any component due to the viewing angle of the accretion disk. Taking this into account would reduce the maximum $E(B-V)$ and improve agreement with the observations.

We conclude that the Netzer AD disk model surrounded by an optically thick dusty torus, with the addition of small amounts of dust outside the BELR, fits well into our line-continuum correlations. Our conclusion that the SMC dust extinction curve, which corresponds well to extinction by dust dominated by small amorphous carbon grains (see Czerny et al. 1995), fits better than the Seaton extinction curve is consistent with previous results that the dust in Seyfert galaxies and quasars may differ from the dust in our Galaxy, showing a depletion of silicates (Czerny, Loska, & Szczerba 1991; Laor & Draine 1993).

4.1.7. *The Torus*

The assumption that quasars have the same dusty torus as the Sy1/Sy2 galaxies (§ 4.1.3) may not be valid. Perhaps the opening angle and radius or thickness of a torus depends on the luminosity of the central engine. More luminous quasars would then have larger opening angles and larger radius/thinner tori. A large torus opening angle would naturally explain the flat slope and large scatter for the carbon C IV and C III] line versus driving continuum correlations. This scenario could also explain why we see the Sy1/Sy2 dichotomy, when there is nothing similar for quasars. However, the other lines would then be too steep for the AD model, so this scenario would require a different emitting region for the carbon lines. This seems contrived and an unlikely possibility given the generally similar behavior of the UV lines.

4.1.8. *LOC Model*

As was mentioned earlier, the majority of existing BELR models have been based on one or two zones of clouds. In recent papers, Baldwin et al. (1995) and Korista et al. (1997) model the BELR from many clouds covering a wide range in distance r from the ionizing source and with a wide range in gas density n_H at each r. The integrated BELR spectrum is determined by integrating over the full distribution function of clouds at all radii and densities. This is called the locally optimally emitting cloud (LOC) model. This model predicts that the integrated spectrum depends only weakly on the shape of the ionizing spectrum, the column density of the clouds, and the cloud distribution with r (see Fig. 2 in Baldwin 1997). This implies that the BELR spectrum is determined more by selection effects than by details of the cloud properties. Since we have concluded that the behavior of the emission lines in our sample is not purely due to photoionization effects, it seems likely that a combination of a BELR based on the LOC model, an AD providing the ionizing continuum, and a distribution of dust external to both AD and BELR would be able to fully describe our sample.

5. CONCLUSIONS

We investigate the relations between various emission-line parameters and continuum parameters in a sample of low-redshift ($z < 1$) quasars. The sample consists of radio-loud and radio-quiet objects for which IR to soft–X-ray SEDs are available and is biased toward AGNs with strong X-ray emission relative to the optical. Eleven newly compiled SEDs and optical spectra for all the quasars are presented. We have measured all the emission-line parameters uniformly to minimize the scatter generally introduced when combining data sets from different techniques and different authors. We use survival analysis that allows for the presence of upper limits.

We find anticorrelations between the line EWs and UV luminosities, i.e., the Baldwin effect, for the Lyα and Hβ lines. Exclusion of narrow-line, low-luminosity AGNs reveals the Baldwin effect also for the C IV and C III] lines. This suggests that NLSy1 objects may have systematically lower carbon EW. We also find a significant correlation between C IV and α_{ox}.

No correlations between the EW and the X-ray luminosity or slope are reported. However, Fe II λ4750 shows a tendency for objects with flat X-ray spectra and/or strong X-ray luminosities to have weak Fe II (which is consistent with Peterson et al. 1981; Phillips 1977; Osterbrock 1977). The anticorrelation between the EW([O III]) and EW(Fe II) (i.e., the first Boroson & Green 1992 eigenvector) is present in our sample.

Correlations between the various parameters for each line were also studied. We confirm the correlations between the FWHMs and EWs of C IV, Lyα, and Hβ lines previously found by Corbin (1991) and Corbin & Boroson (1996), indicating that the HIL and LIL components in the BLR scale similarly with luminosity. This is consistent with both a model where LILs and HILs are formed in the same clouds but in zones of differing ionization, as well as a model where LILs are formed in the atmosphere of an AD, while HILs form in a distinct spherical component.

The continuum-continuum correlations reveal that the peak of the BBB strengthens and perhaps shifts from the EUV into the UV as the luminosity increases. We confirm that the X-rays are systematically lower relative to the optical for higher luminosity objects (Wilkes et al. 1994). However, both high- and low-luminosity objects show a broad range in continuum shapes, and the distributions of SEDs for these subsamples overlap.

We investigate correlations between the line flux and various continuum fluxes, including the driving continuum flux, i.e., the part of the continuum responsible for ionizing each line. While the line-driving continuum correlations are strong, in no case were they the primary line versus continuum correlations. In a pure photoionization scenario this is surprising but can be explained by the presence of dust that reddens both the lines and continuum similarly.

All the above correlations fit into the accretion-disk model of Netzer et al. (1992 and references therein), where an optically thick, geometrically thin AD is composed of two components: a viewing-angle–dependent UV continuum, due to limb darkening and the change in projected surface area, and a viewing-angle–independent X-ray continuum. The model is consistent with our data, as both the predicted EW anticorrelations with UV luminosity and α_{ox} and the lack of correlations with the X-ray continuum are seen in our sample. A quantitative look at the line flux versus continuum flux correlations (i.e., the primary correlations, regression slopes, and scatter) reveals discrepancies that can be explained if dust is present, reddening both the

lines and the continuum. Simulations suggest that the composition of the dust matches that of the SMC rather than our Galaxy, i.e., showing a depletion of silicates (consistent with previous studies: Czerny et al. 1995; Laor & Draine 1993). The slopes of the line flux versus driving continuum flux correlations for C IV and C III] lines are flatter than predicted and with too large a scatter to fit into the AD plus dust model. This can be explained if, as is typical, there is a significant contribution from collisional excitation. The correlation would then be flatter, as only a part of the line flux would be directly related to the ionizing continuum.

We are grateful to Adam Dobrzycki for providing us with the *HST* data, Kim McLeod for precise estimates of starlight for a few objects in our sample, and Ken Lanzetta for the *IUE* Atlas of AGN spectra. We thank Bożena Czerny and Martin Elvis for valuable discussions and the referee for comments that improved the paper. B. J. W., J. C. M., and P. J. G. gratefully acknowledge support provided by NASA through contract NAS8-39073 (ASC). J. K. acknowledges the support of a Smithsonian predoctoral fellowship at Harvard-Smithsonian Center for Astrophysics and KBN grant 2P03D00410. S. M. acknowledges support by NASA grant NAG5-3249 (LTSA) and P. J. G. grant HF-1032.01-92A awarded by the Space Telescope Science Institute, which is operated by the Association of Universities for Research in Astronomy, Inc., under NASA contract NAS5-26555.

REFERENCES

Baker, J. 1997, MNRAS, 286, 23
Baldwin, J. A. 1977, ApJ, 214, 679
———. 1997, in ASP Conf. Ser. 113, IAU Colloq. 159, Emission Lines in Active Galaxies: New Methods and Techniques, ed. B. M. Peterson, F. Z. Chang, & A. S. Wilson (San Francisco: ASP), 80
Baldwin, J. A., Burke, W. L., Gaskell, C. M., & Wampler, E. J. 1978, Nature, 273, 431
Baldwin, J. A., Ferland, G., Korista, K., & Verner, D. 1995, ApJ, 455, L119
Baldwin, J. A., Wampler, E. J., & Gaskell, C. M. 1989, ApJ, 338, 630
Bentley, M., Haves, P., Spencer, R. E., & Stannard, D. 1975, MNRAS, 173, 93P
Boller, T., Brandt, W. N., & Fink, H. 1996, A&A, 305, 53
Boroson, T. A. 1989, ApJ, 343, 9
Boroson, T. A., & Green, R. F. 1992, ApJS, 80, 109
Boyle, B. J., Jones, L. R., & Shanks, T. 1991, MNRAS, 251, 482
Burstein, D., & Heiles, C. 1978, ApJ, 225,40
Coleman, G. D., Wu, C. C., & Weedman, D. W. 1980, ApJS, 43, 393
Collin-Soufrin, S., Dyson, J. E., McDowell, J. C., & Perry, J. J. 1988, MNRAS, 232, 539
Comastri, A., Setti, G., Zamorani, G., Elvis, M., Giommi, P., Wilkes, B. J., & McDowell, J. C. 1992, ApJ, 384, 62
Condon, J. J., O'Dell, S. L., Puschell, J. J., & Stein, W. A. 1981, ApJ, 246, 624
Corbin, M. R. 1991, ApJ, 371, 51
Corbin, M. R., & Boroson, T. A. 1996, ApJS, 107, 69
Corbin, M. R., & Francis, P. J. 1994, AJ, 108, 2016
Crampton, D., Cowley, A. P., & Hartwick, F. D. A. 1990, AJ, 100, 47
Cutri, R. M., Wiśniewski, W. Z., Rieke, G. M., & Lebofsky, M. J. 1985, ApJ, 296, 423
Czerny, B., Loska, Z., & Szczerba, R. 1991, in Physics of Active Galactic Nuclei, ed. W. J. Duschl & S. J. Wagner (Berlin: Springer), 198
Czerny, B., Loska, Z., Szczerba, R., Cukierska, J., & Madejski, G. 1995, Acta Astron., 45, 623
Elvis, M., et al. 1994, ApJS, 95, 1 (E94)
Elvis, M., Green, R. F., Bechtold, J., Schmidt, M., Neugebauer, G., Soifer, B. T., Matthews, K., & Fabbiano, G. 1986, ApJ, 310, 291
Ennis, D. J., & Neugebauer, G. 1982, ApJ, 262, 460
Francis, P. J., Hewett, P. C., Foltz, C. B., & Chaffee, F. H. 1992, ApJ, 398, 476
Green, P. J. 1996, ApJ, 467, 61
Green, P. J., et al. 1995, ApJ, 450, 51
Hyland, A. R., & Allen, D. A. 1982, MNRAS, 199, 943
Isobe, T., Feigelson, E. D., & Nelson, P. I. 1986, ApJ, 306, 490
Kellermann, K. I., Schmidt, M., Shaffer, D. B., & Green, R. 1989, AJ, 98, 1195
Kendal, M., & Stuart, A. 1976, The Advanced Theory of Statistics, Vol. 2 (New York: Macmillan)
Korista, K., Baldwin, J. A., Ferland, G., & Verner, D. 1997, ApJS, 108, 401
Krolik, J. H., & Kallman, T. R. 1988, ApJ, 324, 714
Kuhn, O. 1996, Ph.D. thesis, Harvard Univ.
Lanzetta, K. M., Turnshek, D. A., & Sandoval, J. 1993, ApJS, 84, 109
Laor, A., & Draine, B. T. 1993, ApJ, 402, 441
Laor, A., Fiore, F., Elvis, M., Wilkes, B. J., & McDowell, J. C. 1997, ApJ, 477, 93
Lawrence, A., Elvis, M., Wilkes, B. J., McHardy, I., & Brandt N. 1997, MNRAS, 285, 879
Low, F. J., Cutri, R. M., Kleinmann, S. G., & Huchra, J. P. 1989, ApJ, 340, L1
McDowell, J. C., Canizares, C., Elvis, M., Lawrence, A., Markoff, S., Mathur, S., & Wilkes, B. J. 1995, ApJ, 450, 585
McLeod, K. K., & Rieke, G. H. 1994a, ApJ, 431, 137
———. 1994b, ApJ, 420, 58
Miley, G. K., & Hartsuijker, A. P. 1978, A&AS, 34, 129
Murdoch, H. S. 1983, MNRAS, 202, 987
Mushotzky, R., & Ferland, G. J. 1984, ApJ, 278, 558
Netzer, H. 1985, MNRAS, 216, 63
Netzer, H. 1987, MNRAS, 225, 55
Netzer, H., Laor, A., & Gondhalekar, P. M. 1992, MNRAS, 254, 15
Neugebauer, G., Green, R. F., Matthews, K., Schmidt, M., Soifer, B. T., & Bennett, J. 1987, ApJS, 63, 615
Neugebauer, G., Miley, G. K., Soifer, B. T., & Clegg, P. E. 1986, AJ, 308, 815
Neugebauer, G., Oke, J. B., Becklin, E. E., & Matthews, K. 1979, ApJ, 230, 79
Osmer, P. S. 1980, ApJS, 42, 523
Osterbrock, D. E. 1977, ApJ, 215, 733
Osterbrock, D. E., & Pogge, R. W. 1985, ApJ, 297, 166
Owen, F. N., Porcas, R. W., Mufson, S. L., & Moffett, T. J. 1978, AJ, 83, 685
Owen, F. N., & Puschell, J. J. 1982, AJ, 87, 595
Parley, R. A. 1982, AJ, 82, 859
Penfold, J. E. 1979, MNRAS, 186, 297
Peterson, J. G., Foltz, C. B., & Byard, P. L. 1981, ApJ, 251, 4
Phillips, M. M. 1977, ApJ, 215, 746
Phillips, M. M., Charles, P. A., & Baldwin, J. A. 1983, ApJ, 266, 485
Pogge, R. W., & Peterson, B. M. 1992, AJ, 103, 1084
Pooley, G. G., & Henbest, S. N. 1974, MNRAS, 169, 477
Pounds, K. A., Done, C., & Osborne, J. P. 1996, MNRAS, 277, 1430
Prévot, M. L., Lequeux, J., Maurice, E., Prévot, E., & Rocca-Volmerange, B. 1984, A&A, 132, 389
Puchnarewicz, E. M., et al. 1996, MNRAS, 281, 1243
Rawlings, S., Lacy, M., Sivia, D. S., & Eales, S. A. 1995, MNRAS, 273, 821
Robertson, J. G. 1986, PASP, 98, 1220
Robson, E. I., Gear, W. K., Smith, M. G., Ade, P. A. R., & Nolt, I. G. 1985, MNRAS, 213, 355
Romanishin, W., & Hintzen, P. 1989, ApJ, 341, 41
Sanders, D. B., Phinney, E. S., Neugebauer, G., Soifer, B. T., & Matthews, K. 1989, ApJ, 347, 29
Seaton, M. J. 1979, MNRAS, 187, 73P
Shastri, P., Wilkes, B. J., Elvis, M., & McDowell, J. 1993, ApJ, 410, 29
Sitko, M. L., Stein, W. A., Zhang, Y.-X., & Wiśniewski, W. Z. 1982, ApJ, 259, 486
Smith, E. P., Heckman, T. M., Bothun, G. D., Romanishin, W., & Balick, B. 1986, ApJ, 306, 64
Sprayberry, D., & Foltz, C. B. 1992, ApJ, 390, 39
Steppe, M., Salter, C. J., Chini, R., Kreysa, E., Brunswig, W., & Perez, J. L. 1988, A&AS, 75, 317
Swarup, G., Sinha, R. P., & Hilldrup, K. 1984, MNRAS, 208, 813
Tananbaum, H., Avni, Y., Green, R. F., Schmidt, M., & Zamorani, G. 1986, ApJ, 305, 57
Taylor, G. L., Dunlop, J. S., Hughes, D. H., & Robson, E. I. 1996, MNRAS, 283, 930
Tytler, D., & Fan, X.-M. 1992, ApJS, 79, 1
Walter, R., & Fink, H. H. 1993, A&A, 274, 105
Wampler, E. J., Gaskell, C. M., Burke, W. L., & Baldwin, J. A. 1984, ApJ, 276, 403
Webster, R. L., Francis, P. J., Peterson, B. A., Drinkwater, M. J., & Masci, F. J. 1995, Nature, 375, 469
Wilkes, B. J., & Elvis, M. 1987, ApJ, 323, 243
Wilkes, B. J., Elvis, M., & McHardy, I. 1987, ApJ, 321, 23
Wilkes, B. J., & McDowell, J. C. 1995, in ASP Conf. Ser. 61, Astronomical Data Analysis and Software Systems III, ed. D. Crabtree, R. Hanisch, & J. Barnes (San Francisco: ASP), 423
Wilkes, B. J., Tananbaum, H., Worrall, D. M., Avni, Y., Oey, M. S., & Flanagan, J. 1994, ApJS, 92, 53
Williams, O. R., et al. 1992, ApJ, 389, 157
Wills, B. J., Brotherton, M. S., Fang, D., Steidel, C. C., & Sargent, W. L. W. 1993, ApJ, 415, 563
Zamorani, G., Marano, B., Mignoli, M., Zitelli, V., & Boyle, B. J. 1992, MNRAS, 256, 238
Zheng, W., Kriss G. A., & Davidsen, A. F. 1995, ApJ, 440, 606
Zheng, W., & Malkan, M. A. 1993, ApJ, 415, 517
Zheng, W., & O'Brien, P. T. 1990, ApJ, 353, 433